2002-W01_optimalisatie-ronde-nabezinktanks-modelproeven

stowa

Stichting Toegepast Onderzoek Waterbeheer

Optimalisatie van ronde nabezinktanks

Modelproeven

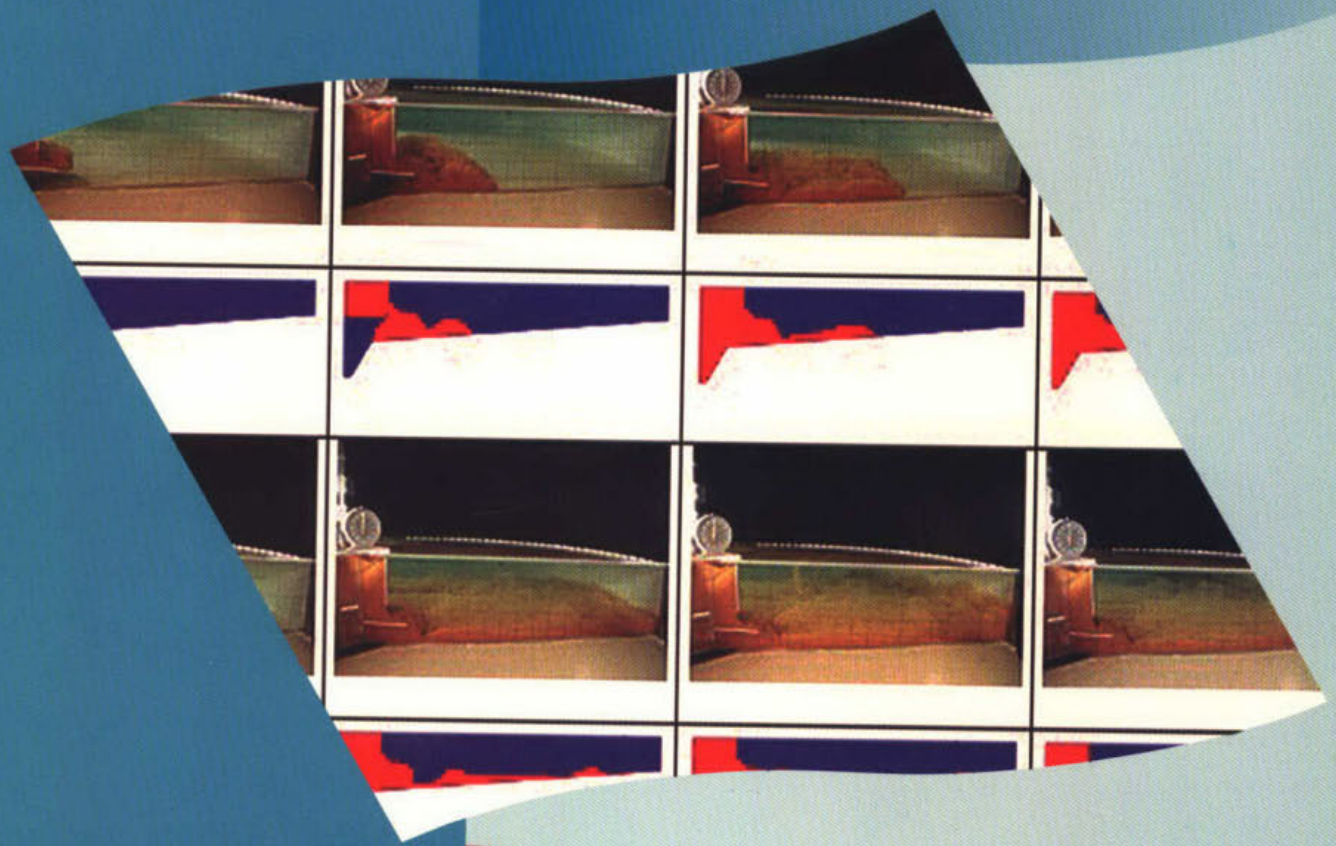

2002 W01

stowa

Stichting Toegepast Onderzoek Waterbeheer

Optimalisatie van ronde nabezinktanks

Modelproeven

Arthur van Schendelstraat 816
Postbus 8090, 3503 RB Utrecht
Telefoon: 030 - 232 11 99
Fax: 030 - 232 17 66
E-mail: stowa@stowa.nl
http://www.stowa.nl

Publicaties en het publicatie-overzicht
van de STOWA kunt u uitsluitend bestellen bij:
Hageman Fulfilment
Postbus 1110
3300 CC Zwijndrecht
Telefoon: 078 - 629 33 32
fax: 078 - 610 42 87
E-mail: hff@wxs.nl
o.v.v. ISBN- of bestelnummer
en een duidelijk afleveradres.

ISBN 90-5773-176-2

2002 W01

Colofon:

Utrecht, 2002

Uitgave:
STOWA, Utrecht

Uitvoering:
Institute for Hydrodynamics
University of Karlsruhe

Projectteam:
Martin Armbruster
Wolfgang Rodi

Begeleidingscommissie:
Tom Wouda (voorzitter)
Bonnie Bult
Jeroen Kluck
Freek Kramer
Paul Roeleveld
Pieter Stamperius
Han Winterterp

Foto omslag:
Gedrag van synthetisch slib in een schaalmodel nabezinktank

Druk:
Kruyt Grafisch Advies Bureau

STOWA rapportnummer 2002-W01

ISBN nummer 90-5773-176-2

1 Introduction 3

2 Physical Model of the Secondary Settling Tank 4

2.1 Initial Geometry and Scaling of the Model Parameters 4

2.1.1 The Model Set-Up 4

2.1.2 Suspension 6

3 Measurement Probes 11

3.1 Velocity Measurement 11

3.2 Concentration Measurement 12

3.3 Accuracy and limits of the Probes 14

3.4 Control and security devices 15

4 First tests and Modifications of Set-up 17

4.1 Tests in the Model with its Original Set-up 17

4.2 Modifications of Set-up 17

4.2.1 Measures to overcome Internal Friction of Particles 18

4.2.2 Changes to Scraper 19

5 Measurements in the Full Circular Tank 22

6 Test with Iron Hydroxide in the Suspension 27

7 Final Measurements 30

7.1 ¾ Tank for Unsteady Starting Phase 30

7.2 Test Cases 32

7.3 Analysis of the Measurements 34

7.3.1 Concentration Measurements 34

7.3.2 Suspension Front Spread 36

7.4 Comparison with Computations 41

7.4.1 Case B 43

7.4.2 Case D 44

7.4.3 Case A 45

7.4.4 Case C 46

8 Conclusions 50

9 References 51

1 Introduction

As item 2.2 (verification of numerical model) of the STOWA project "Modelling of circular secondary sedimentation tanks" measurements were to be carried out in a laboratory tank against which the numerical model developed at the Institute for Hydromechanics could be validated. For this purpose, a 1:10 model of a typical Dutch secondary sedimentation tank (SST) was built in the water laboratories of the Institute for Hydromechanis, University of Karlsruhe. It was planned to run this model mainly under steady conditions and to measure profiles of sediment concentrations as well as flow velocities, but at a later stage also measurements for unsteady situations were intended. Changes in load, geometry of the inflow and sludge removal system and in height of the side water baffle were intended in order to gain a set of data for a range of situations for which the numerical model could then be validated. In the planning stage, different materials such as glass beads, plastic beads or special artificial sludge and clay were considered and discussed as possible model suspensions. Finally, monodisperse plastic beads named Lewatit delivered by the Bayer Company were chosen. During the initial tests it was found that the flow properties of these particles were not as expected as they stuck to the bottom once they had settled there and the sludge scraper was not able to remove the settled particles to such an extent that the sedimentation tank systems could have come to an equilibrium state as planned; rather the tank filled up with particles and the whole system broke down. In order to overcome this problem a number of modifications to the experimental system were considered and tested such as a change of the geometry of the sludge removal zone, geometry of the scrapers, speed of the scrapers, smoothness of the bottom. Further, the suspension was modified by introducing iron hydroxide flocks and polymers to reduce the internal friction between the particles. However, all these measures did not produce the desired result of obtaining a steady-state situation in the tank without having this totally filled up by the particles. In addition, difficulties were also encountered with the measurement probes, mainly because of the high concentrations and low velocities in the model tank. So it was decided in the end to give up the plan to obtain detailed measurements under steady conditions and to switch to a simpler system in which only the initial phase of the unsteady filling process starting from an empty tank was observed optically through transparent side walls of a ¾ sector of the full circular tank. This situation was also simulated by the numerical model. This report summarises the various attempts and describes the difficulties encountered and it presents the final results of the unsteady tests for the initial filling period and compares them with the numerical calculations.

2 Physical Model of the Secondary Settling Tank

2.1 Initial Geometry and Scaling of the Model Parameters

2.1.1 The Model Set-Up

The model was designed as a 1:10 scale model of a circular secondary settling tank with the following main dimensions which are typical for Dutch clarifiers:

	Prototype	***Scale Model***
Diameter	*40 m*	*4 m*
Side Water Depth	*2 m*	*15 – 25 cm*
Slope of Bottom	*1:12 (4.8°)*	*1:12 (4.8°)*
Height of Scraper		*1.0 cm – 8.0 cm*
Position Horizontal Deflection Baffle		*Adjustable*
Distance Vertical Deflection Baffle to Horizontal Deflection Baffle		*Adjustable*

The basic geometry of the model is shown in Fig. 2.1. Initially a single arm scraper was installed (not shown in Fig. 2.1 but in Fig. 4.4a).

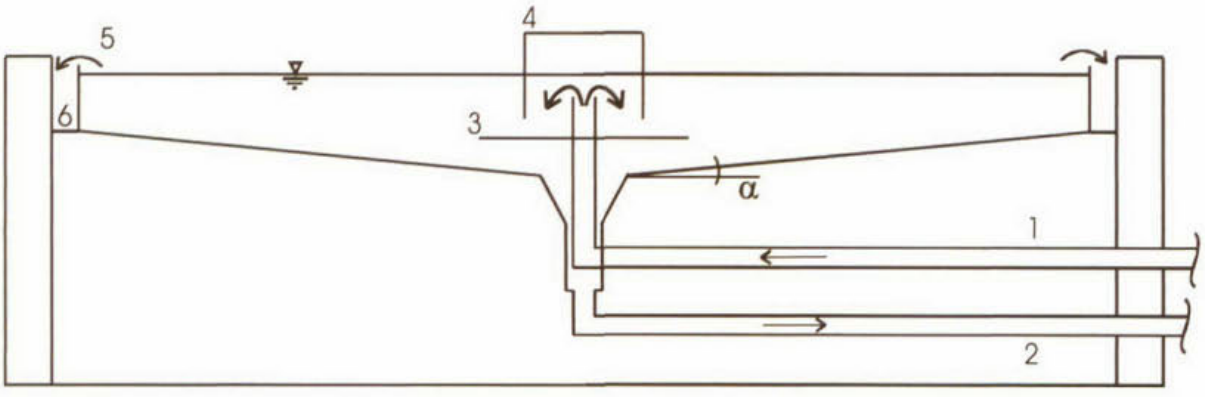

Fig. 2.1 *Settling Tank with:* *1 Inlet* *2 Sludge removal* *3 Hor. Deflection Baffle* *4 Vert. Deflection Baffle* *5 Triangular Weirs* *6 Gully for Clear Water*

It was planned to run the model with different geometric set-ups:

- with or without horizontal deflection baffle
- different gap sizes between horizontal and vertical deflection baffle as well as with
- different side water depths varying between 15 cm and 25 cm (see Fig. 2.3d)

as well as with different loadings like

- dry weather case
- storm water case and
- transient situations

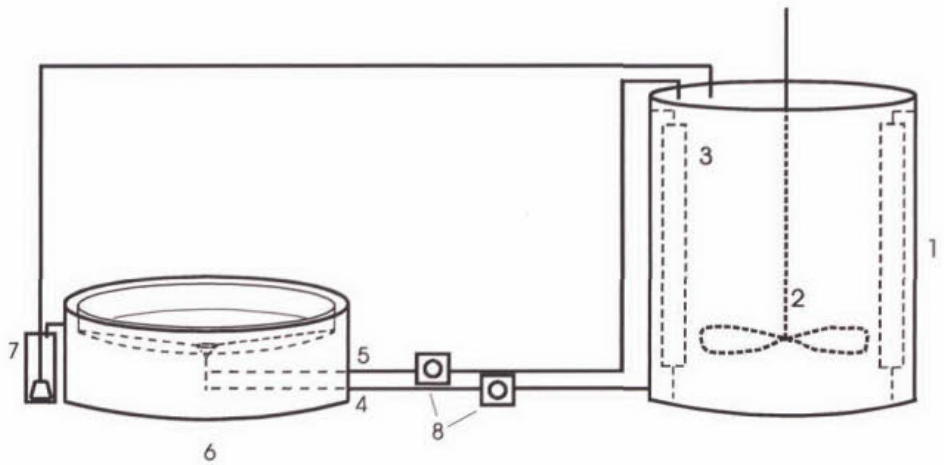

Fig. 2.2 *Sketch of the model with:*

1 Stirring Tank
2 Stirrer
3 Mixing Paddles
4 Inlet pipe
5 Recirculation Pipe
6 Settling Tank
7 Water Collecting Tank
8 Rotary Lobe Pumps

a) Base of the Model

b) Concentric Inlet/Sludge Hopper device

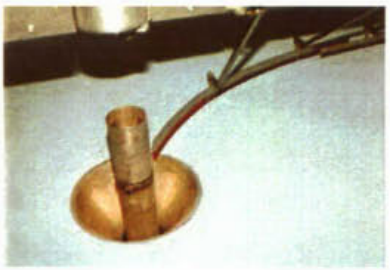

c) Concentric Inlet/Sludge Hopper finished tank

d) Different Adjustable Side Water depths

e) Inlet configuration

f) triangle edged weirs for clear water outlet

g) Rotary Lobe Pumps for Suspension

h) Pipe Network for Inflow and Recirculation

i) In the Foreground the Drive of the Scraper moving on a Circular Rail. In the Background the Stirring Tank

Fig. 2.3 *Initial set-up of the Laboratory SST Model*

2.1.2 Suspension

Activated Sludge is not scalable with all its properties. The particle size as well as its settling behaviour is dependant on a lot of parameters determined by the waste water treatment plant such as waste water composition, oxygen content, detention time, which cannot be modelled in a laboratory. The most important features with respect to the numerical simulations, i.e. the buoyancy effect on the flow and the (hindered) settling of particles however can be reproduced in scale models. Laboratory models have the advantage that they can be run under well controlled boundary conditions like for temperature, flow rate, and sludge conditions. Hence, a substitution of the activated sludge by a model sludge was attempted.

Former works report about modelling density driven flows in settling tank models e.g. with saltwater, clay, sand, glass spheres or flocculent particles.

Scaling

A physical settling tank model has to fulfil certain similarity laws, which are

- The flow has to be turbulent, i.e. the Reynolds Number

  $$\mathrm{R} = \frac{U \cdot H}{\nu},$$

  defined via the mean or the jet velocity U, the mean tank height or the bottom jet height H and the viscosity of the fluid ν has to be large enough, i.e. larger than 1000, the limit for turbulent density current conditions (Simpson, 1987).

- The ratio of momentum to buoyancy forces, represented by the densimetric Froude number

  $$F_D = \frac{U}{\left(\frac{\Delta\rho_0}{\rho} gH\right)^{1/2}},$$

  has to be the same as in the prototype.

Here g is the gravitational acceleration, ρ the density of pure water and $\Delta\rho_0$ the density difference between inflow and pure water, derived from the inlet concentration C_0 by

$$\Delta\rho_0 = C_0 \frac{\rho_P - \rho}{\rho}$$

Where ρ_P is the density of the sludge particles.

- the magnitude of settling velocities related to a typical mean flow velocity via the Hazen number

  $$\mathrm{Ha} = \frac{V_S \cdot L}{U \cdot H}$$

  has to be similar

- at the inlet of the tank the volume fraction of the settling matter has to be at least $\phi = 15\ \%$ Vol. to assure the phenomena of hindered settling in the sludge bed (Mandersloot et. al., 1986).

These demands lead to different possible solutions which are presented in Tab. 2.1. The Reynolds- and Froude Numbers listed in this table are computed for mean values of velocities and total water depths directly at the inlet and at two third of the diameter of the tank.

Material	Scale	Density ρ [kg/m^3]	Inlet Concentration X_0 [kg/m^3]	Surface Load q_A[m/h]	Volume Fraction [1]	Diameter d_p [µm]	Settling Velocity (hindered) V_H [mm/s]	Reynolds Number R [1]		Froude Number Fr_D [1]		Hazen Number V_H/q_A Ha [1]
								Inlet	2/3 R	Inlet	2/3 R	
Act. Sludge	1:1	1450	3.3	0.74	0.5	5600	0.5	25000	3100	0.219	0.011	2.43
$Fe(OH)_3$	1:10	3200	1	0.74	0.23	380	0.07	2500	310	0.843	0.042	0.34
Plastic beads	1:10	1050	200	0.74	0.19	210	0.5	2500	300	0.215	0.011	2.5
Glass beads	1:13	2500	400	2.96	0.26	80	2	6700	820	0.208	0.1	2.5

Tab. 2.1 *Table of Different Sludges and their Characteristic Numbers R, Fr_D, Ha, provided by J. Krijgsman (1996)*

With respect to these similarity conditions a plastic material from Bayer (Leverkusen), named "Lewatit" was chosen. The main advantage of the Lewatit particles over e.g. BASF polystyrene (Fig. 2.4 d) is that they are nearly monodisperse, i.e. the size of all the particles is almost exactly 230 µm (Fig. 2.4 a,b), the density is $\rho_P = 1050$ kg/m^3. Only some bigger conglomerates of particles had to be sifted out (Fig. 2.4 c). This fact makes it easier to perform numerical simulations since the total fraction of settleable matter does not have to be divided into sub-fractions of different sizes resulting in different settling velocities

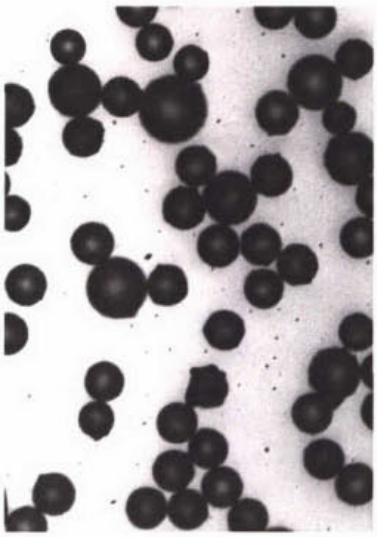

a) Looking at Lewatit with a Microscope

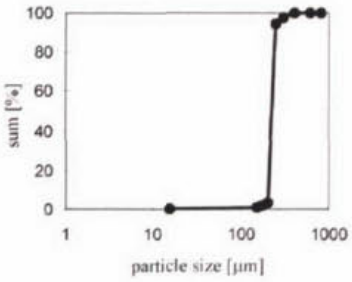

b) Monodispers Size Distribution of Lewatit

c) Sifting of the Lewatit Particles

d) Flow tests with BASF polystyrene particles

Fig. 2.4 *Model Sludge: Pure Lewatit*

Settling Velocity of Lewatit

Following Mandersloot et. al. (1986) the settling velocity of particles in hindered settling conditions is a function of the local concentration V_s=f(C) with $v_s = C_1 \cdot (1-\Phi)^{C_2}$.

Deriving the constants C_1 and C_2 from measurements carried out with the Lewatit particles (Fig. 2.5) leads to

$$v_s = 1{,}286(1-\phi)^{4{,}7826} \qquad (2.1)$$

(see Fig. 2.6) for the given particles.

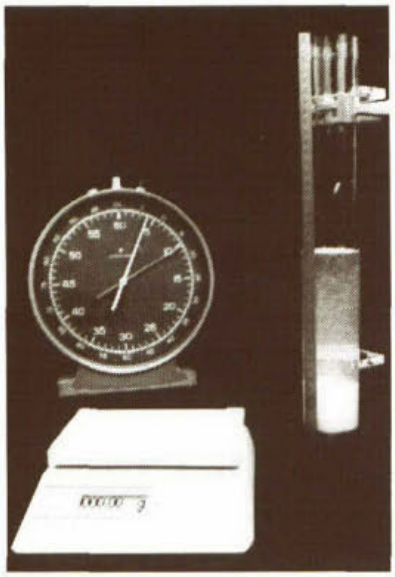

a) Measurement of Settling Velocities

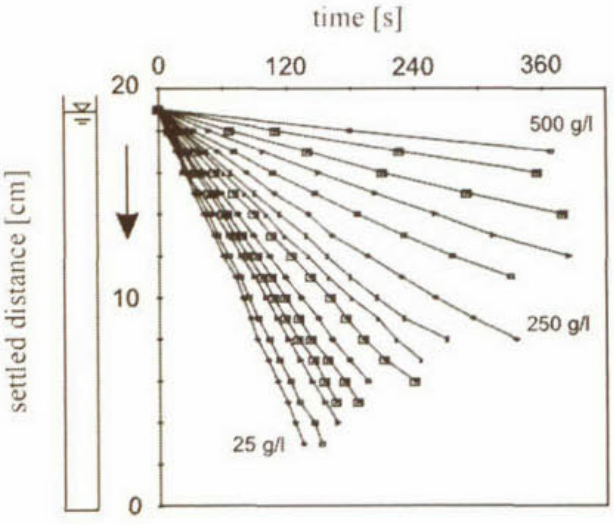

b) Position of the Blanket of the layer of settled particles for different Concentrations as a Function of the elapsed settling time

Fig. 2.5 *Settling Velocity Measurements*

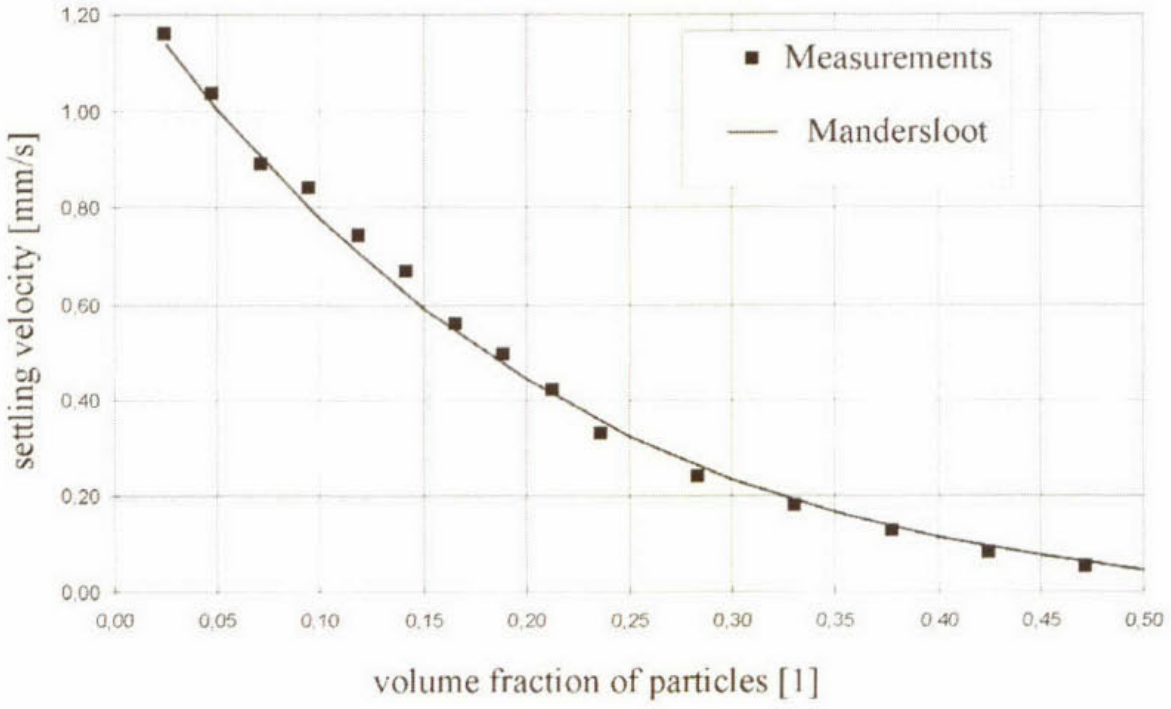

Fig. 2.6 *Settling Velocity Measurements. Mandersloot Settling Function $V_s=f(C)$ derived from measurements shown in Fig. 2.5*

3 Measurement Probes

The nature of the flow in a settling tank generally and in the laboratory model with the chosen suspension especially implies – due to regions with very high concentrations and turbidity and due to rather low velocities – very severe conditions with respect to the measurement probes.

3.1 Velocity Measurement

Most of the usual probes for laboratory or field velocity measurements like **propellers, pitot tubes, and thermoelectric anemometers** are only suitable for

- higher mean velocities and
- lower concentrations

than we have in the model settling tank or have a serious drift (e.g. the electro-magnetic type probe, Fig. 3.3 c). **Laser Doppler Anemometers** that can be used for low velocities were also tested in a turbid flow but failed at suspension concentrations greater than 4 g/l whereas the planned inlet concentration was 200 g/l.

Following a suggestion of Prof. Steven Vogel (Duke University, North Carolina) a home-made probe with very small **thermistors** was tested whose construction details are presented in his book "Life in Moving Fluids" (Vogel, 1981). Due to construction problems in the workshop this technique failed already during the calibration phase.

In another test, a probe measuring travel time of an **electrolytic tracer** was examined. Generally such a method works as follows: electrodes measuring conductivity are placed in a flow field. At some position with known distance L from the electrodes a fluid with different conductivity but same density is introduced into the fluid and the time τ between the release of the tracer and its detected arrival at an electrode is measured. This employs an **autocorrelation method**.

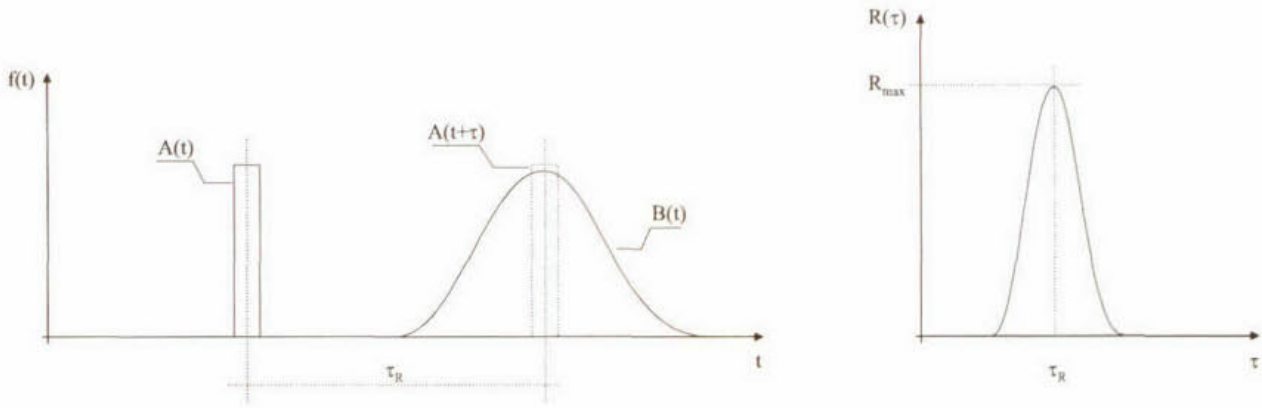

Fig. 3.1 *Autocorrelation*

A function A = f(t) representing the release of the tracer e.g. via a current pulse driving a valve and a second function B = f(t) representing the measured conductivity at the electrodes have to be defined. The first and second derivation of an autocorrelation function dependent on the travel time of the tracer R = f(τ) with

$$R(\tau) = \int \left(A(t+\tau) \cdot B(t) \right) dt$$

then lead to the maximum R(τ) representing the travel time τ_R.

Extensive tests of the method showed on one hand that it principally works but that on the other hand there would have been too many parameters to be controlled to use it in a turbidity flow. For this reason, its use in the lab model was given up.

The probe finally used is the so-called "Sontek **Acoustic Doppler Velocimetry**" probe (ADV). It uses ultrasonic technique to measure velocities in flows carrying a minimum of turbidity since it needs backscattering particles in the flow (Fig. 3.3 a,b). With Lewatit suspension it was found to work up to a concentration of approx. 50 g/l. The probe can measure velocities down to a few millimetres per second. Average values of the velocities measured with the ADV probe are reasonable whereas quantities of turbulence intensities appeared to be overestimated in comparison with LDA measurements.

3.2 Concentration Measurement

Due to the high concentrations and resulting turbidity commonly used techniques like **ultrasonic probes** or probes determining the **backscattering light** or other **optical methods** appeared not to be suitable.

ERSC

The only probe which would have worked in the Lewatit suspension is the "**Electro-Resistance Type Sediment Concentration Meter**" (ERSC; Ulizka,1989). This probe measures conductivity. Two parallel conductors provided with an alternating current of ±10 V form an electrical field in the water. For clear water this field is not disturbed. As soon as non-conducting particles enter, the field starts to be deformed and consequently the conductivity is reduced. This change, which is nearly linearly proportional to the concentration, is measured as a resistance difference with respect to a reference probe situated in clear water via a measurement bridge and an amplifier (Fig. 3.2).

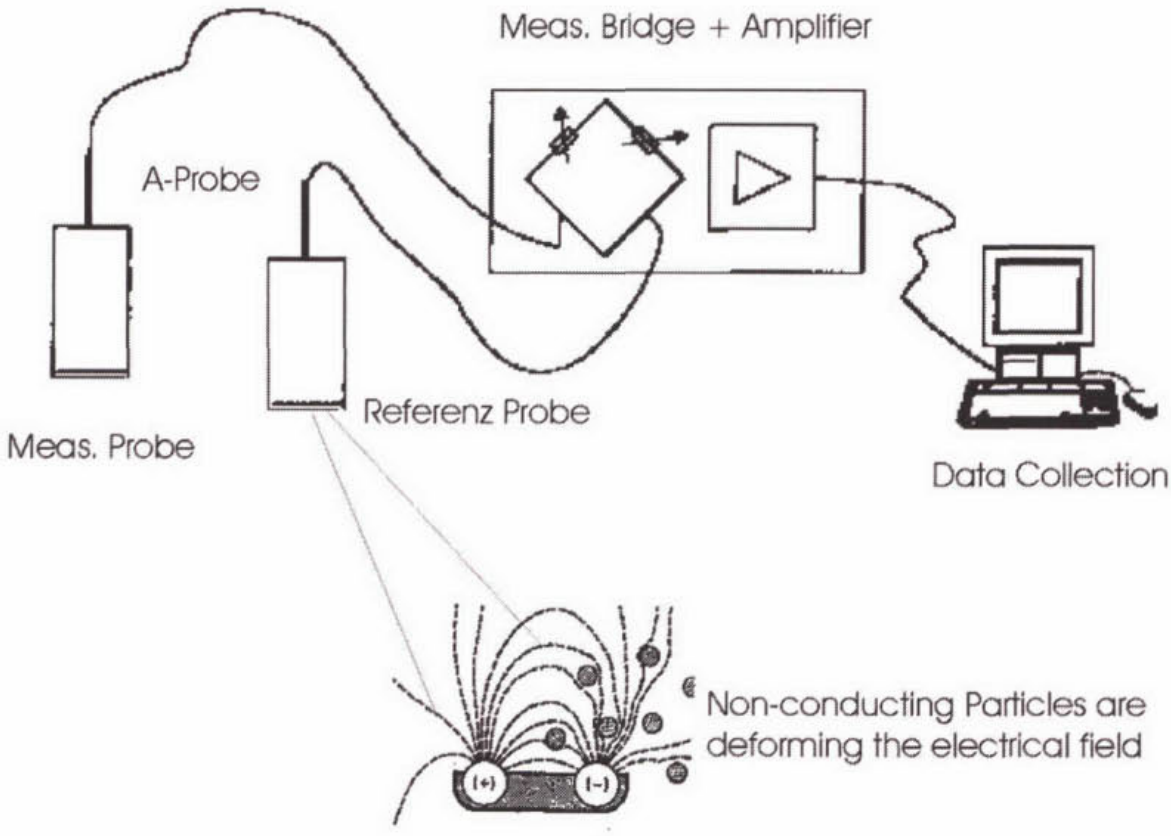

Fig. 3.2 *Working Principle of the Concentration Probe*

Variations to the shape of the ERSC

In first tests this probe was used as a measurement harp with 4 probe tips as described in Ulizka (1989) (Fig. 3.3 f). This would have made it possible to measure a complete profile at once. In practice this failed since it turned out to be too complex to calibrate all four probes together. For this reason finally only single tip probes were used.

A second variation was the shape of the probe. To enable measurements below the horizontal deflection baffle the probe tip was bent by 90° (Fig. 3.3 e).

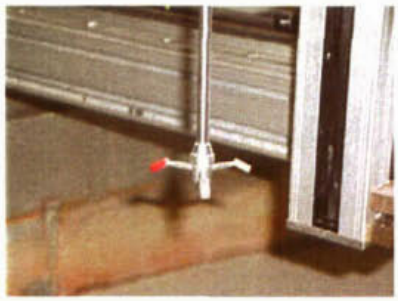

a) 3-D Probe Tip of the ADV Velocity Probe

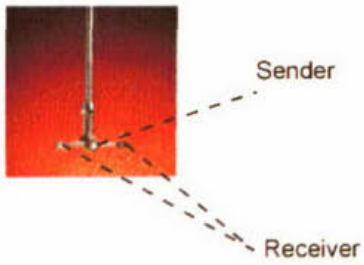

b) Tip of the ADV probe.

c) Electro-magnetic Probe Tip

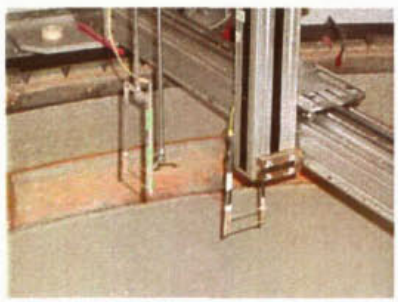

d) ADV+ERSC Probe Tips with ERSC Reference Tip

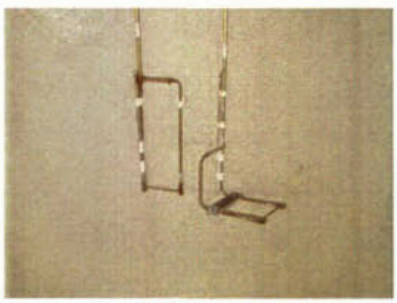

e) ERSC Variation with bent Probe Tip

f) ERSC Variation 4 Channel Harp

Fig. 3.3 *Different Velocity and Concentration Probes*

3.3 Accuracy and limits of the Probes

ADV-Probe

With the ADV probe it was possible to measure velocities down to some millimetres per second with reasonable results. This worked however only when the flow provided the measurement point with sufficient backscattering particles. For the first measurements this was the case at any point of the supernatant water whereas the concentration in the suspension was too high to measure velocities. There the backscattered signal was totally absorbed by the particles before it reached the receiver.

ERSC-Probe

The use of the ERSC probe was only useful in pure Lewatit suspension. In this suspension it was possible to find a quasi-linear calibration curve. For boundaries which limit the extent of the electrical field, however, the results are influenced by the presence of the boundaries (Fig. 3.4). Measurements directly underneath the horizontal deflection baffle had to fail totally

since this device is built out of steel which dramatically reduces the electro-resistance in the measurement volume.

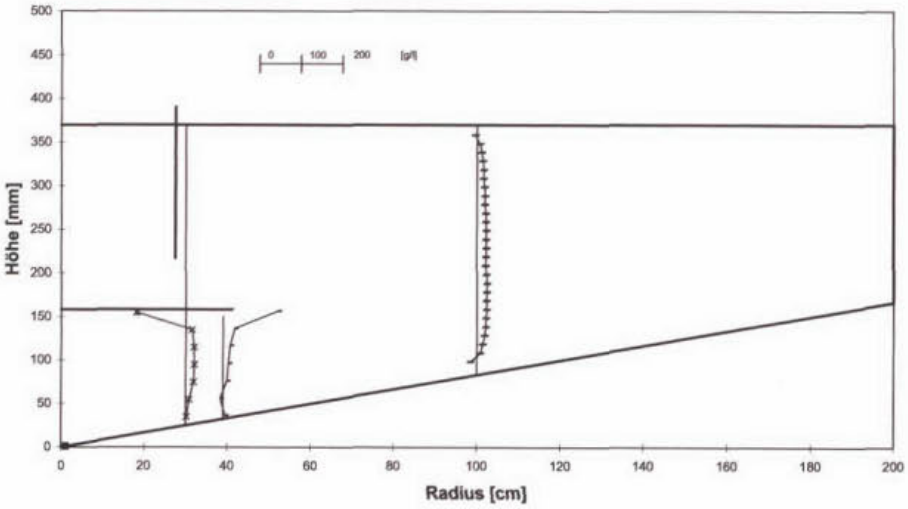

Fig. 3.4 *ERSC-Dependency on Boundaries (Clear Water Calibration in the Model)*

3.4 Control and security devices

In order to induce the flow of the particles to the central sludge hopper, five scrapers with increased size and revolution speed had to be introduced into the tank in a later version of the set-up, leading to the situation that not only once an hour but up to twenty times an hour a scraper, which could damage the probes, passed a measurement point. For this reason it was necessary to install a complex system of security devices avoiding a collision of the scraper blades with a probe tip. Different sensor needles coupled with switches connected to the probe driving motors assured that the measurement probes could not be destroyed by accident.

Other sensors placed at the circumference of the tank started and stopped measurements at points between the scrapers dependent on the actual position of the scrapers.

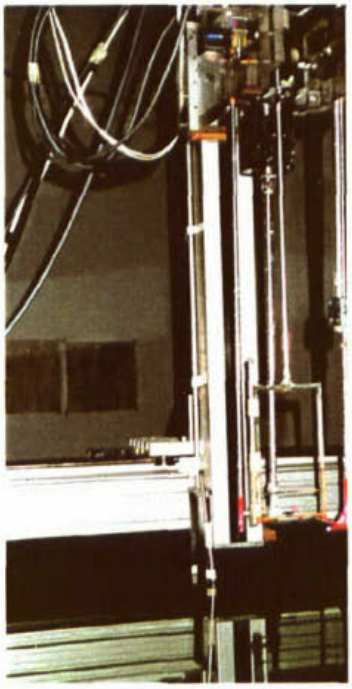

a) ADV and ERSC Probe with Sensor Sticks (Red Tips)

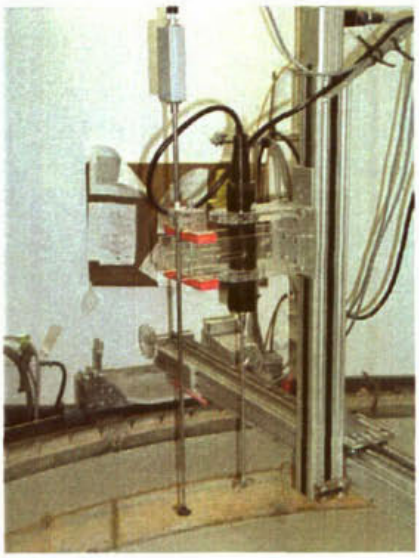

b) Velocity Probes for Final Measurements

Fig. 3.5 *Measurement Bridge with Motor driven Support on a Vertical Stem carrying (a) for the first measurements the ERSC Concentration Probe as well as the ADV Velocity Probe and in (b) two different velocity probes (ADV and Electromagnetic Probe)*

4 First tests and modifications of set-up

4.1 Tests in the Model with its Original Set-up

The first tests with the chosen suspension of Bayer Lewatit particles and an initial inlet concentration of $C_{in} = 200$ g/l showed a rapid failure of the model. The particles settled and stuck to the bottom and the thickness of the layer of settled particles increased continuously. Finally the scraper pushed the top of the layer of settled particles above the water surface. The amount of recirculated particles was reduced drastically so that the concentration in the stirring tank was reduced to low values. At the end of this unsteady process most of the particles were stored in the model tank (Fig. 4.1).

a) Lewatit particles sticking at the inlet of the model

b)Cross-section of the Particle Bed during first Tests

c) View into totally filled Model

Fig. 4.1 *Model is filled totally with Particles*

4.2 Modifications of Set-up

To overcome the problems with the non-moving settled particles different measures were tested.

4.2.1 Measures to overcome Internal Friction of Particles

The tendency of the particles to build up a much too massive particle layer rather than flowing like real activated sludge was obviously a result of a too high internal friction of the particles combined with a too high bottom friction of the settled material. Different – finally unsuccessful – measures to overcome these problems were discussed and tested:

- First of all flow conditions were improved by redesigning the recirculation zone i.e. forming the lower part of the deflection baffle in a streamlined form (Fig. 4.2 a) and by increasing the gap size between the horizontal deflection baffle and the bottom of the model to increase the flow area.

- A second measure was to paint the model with a special coating leading to an extremely smooth bottom.

- A "moving bottom" to overcome bottom friction was tested in a sector of the tank (Fig. 4.2 b,c). For this a grid was mounted on a frame. This device was oscillated by hand on the bottom. It was found out that at a certain minimum frequency of movement it was possible to come to a stationary situation with a reasonable height of the particle layer. But a further increase of the speed of grid movement decreased the height of the particle layer further so that the build-up of the particle layer clearly was dependent on the frequency of the moving grid rather than determined by the flow situation.

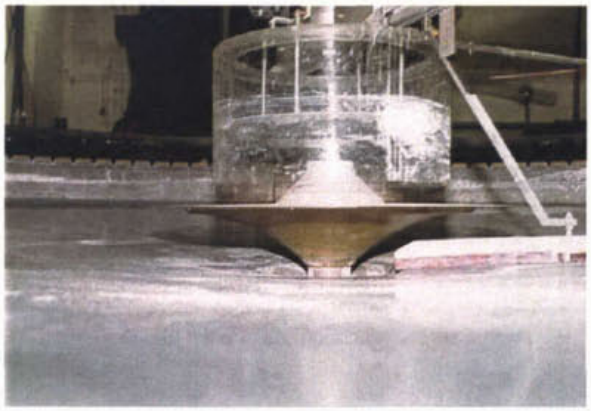

a) Optimized Streamlined Design of the Recirculation Zone

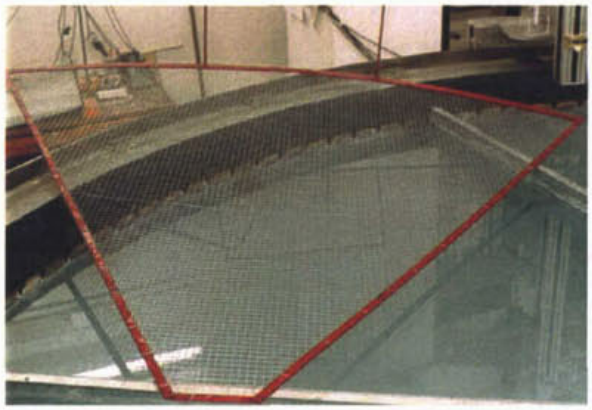

b) "Moving bottom" Device

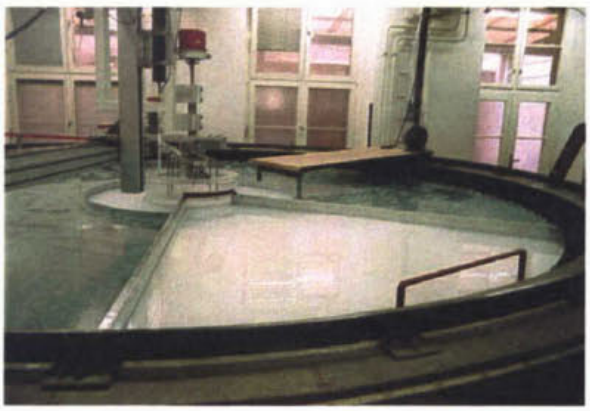

c) Test Measurement with the Moving Bottom Device in a sector of the Tank.

***Fig. 4.2** Pictures of some tested Measures and/or added Devices to Overcome the Problems*

4.2.2 Changes to Scraper

The scraper was redesigned in different ways. First of all a bigger scraper blade height together with a much more bent and therefore longer scraper was tested.

Since this measure did not solve the problem, additionally the scraper speed was increased. As a starting value a speed of one revolution per hour (rph) – which was the speed of the initial model design – was chosen and then gradually increased. With an approx. twenty fold higher speed (i.e. 20 rph or one revolution in three minutes) the system came into balance for a dry weather case (q_A =0.3 m/h). The swirl however became the dominant motion in the flow at this rate of revolutions. Velocities of the order of 0.1 – 1 cm/s in the main flow direction were superposed by 50 cm/s swirl velocity. So it was finally decided to reduce the rotations to 4 rph but at the same time increase the number of scrapers from one to five.

Due to the increased speed of the scraper it was no longer possible to leave the drive of the scraper on the circular rail around the model (since the same rail had to carry the bridge for the measurement devices, see Fig. 4.3). Before this change, it was only once per hour that the car of the drive of the scraper (Fig. 4.4a), travelling continuously on the same circular rail around the model as the stationary car of the measurement bridge reached the latter so that the measurement bridge, when directly in front of the scraper had to be moved one revolution to be again far away from the car of the scraper. Moving it every quarter of an hour however would have made measurements impossible.

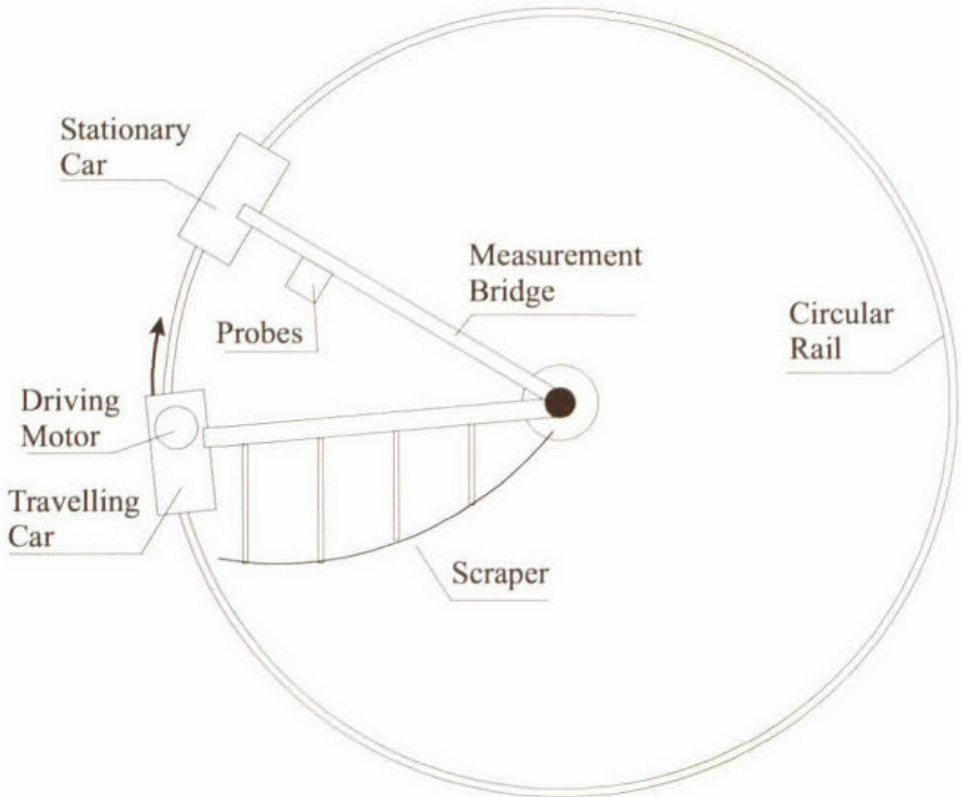

Fig. 4.3 *Principle of the Initial Set-up of Scraper Drive and Measurement Bridge. One Circular Rail around the Model carries both the Car of the Measurement Bridge and the Car of The Scraper Drive.*

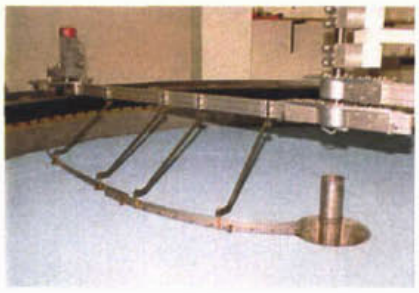

a) Initial Set-Up with Scraper Bridge driven by a Motor on a Car Moving on a Rail

b) Five Scrapers with higher Scraper Blades and an increased Length

c) Detail of the Inner Support of the Scrapers (Changed later due to too high friction)

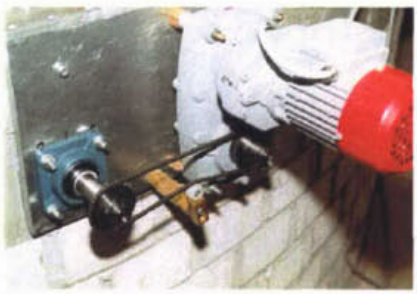

d) Final Set-Up of the Stationary Drive

e) Inner Part of the Drive. First Version with a Friction Wheel

f) Inner Part of the Drive. Final Version with a Gearwheel and chain

Fig. 4.4 *Modifications to the scraper and its Drive*

5 Measurements in the Full Circular Tank

After the various reconstructions of the laboratory tank and all its technical parts the system seemed to work properly. The aim of the following measurements should have been to examine the influence of changes to the load of the tank and the geometry of the inlet on the flow situation and on the efficiency of the system. For a first set of measurements four different cases with suspension and one clear water case were chosen. Besides variations of the load also experiments with and without a cover over the sludge hopper in form of a horizontal deflection baffle were carried out (Tab. 5.1). In a later phase, the outlet configuration (i.e. the side water depth) should have been varied and finally unsteady loadings should have been examined.

Case	Hor. Deflection Baffle	q_A [m/h]	R [Q_{rec}/Q]	C_{in} [g/l]
Clear Water	with	0.37	1.54	0
S4	with	0.34	1.66	200
D4	with	0.23	1.75	200
S5	without	0.40	1.37	90
D5	without	0.26	1.56	130

Tab. 5.1 *Specification of different test cases*

It was clear from observations that the thickness of the surface of the layer of settled particles would not be constant but considerably larger at the locations of the scraper (see Fig. 5.1). For this reason, probes could at one point sometimes be in the layer of settled particles and sometimes outside the layer. Taking mean values over a longer period of time would therefore mean that one would have pseudo values of measured magnitudes mixed from two totally different situations like for instance full settled particle concentration and zero concentration. The measurement strategy was therefore to split the total measurement time, i.e. the time after a leading scraper passed a measurement point until the following scraper came near this point, into a starting, a middle and an end interval of 15 seconds each and using only the results of intervals for which it was clear that the probes were within the particle layer all of the time or above the particle layer all of the time respectively.

Fig. 5.2 shows the evaluation principle: the total measurement time at e.g. profile point 25 at a radius of R = 800 mm lasted from approx. 30 seconds after the leading scraper had passed to approx. 135 seconds after the leading scraper had passed, i.e. the time the following scraper

came near. The green parts of the graphs represent the three intervals during which the measurements were accepted whereas the yellow parts are times of measurement not further used.

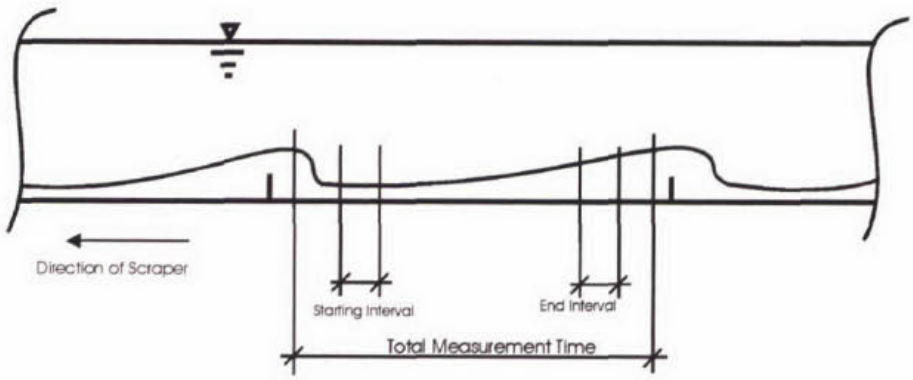

Fig. 5.1 *Variable Thickness of Settled Particle Layer (in Circumferential Direction).*

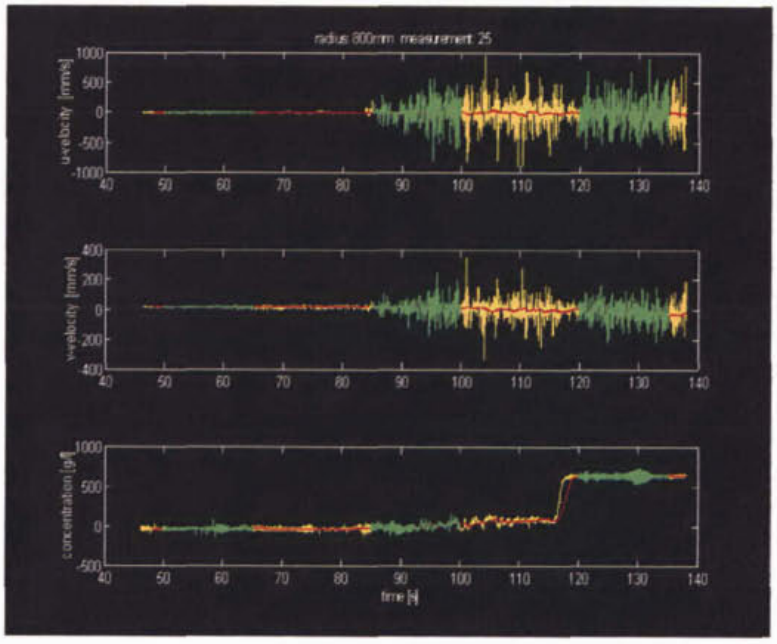

Fig. 5.2 *Output of the evaluation program for measurement signals*

A first measurement was carried out with clear water. All the control and safety functions for the measurement devices could be checked in this test case. The results for the measured velocities together with derived streamlines are presented in Fig. 5.3.

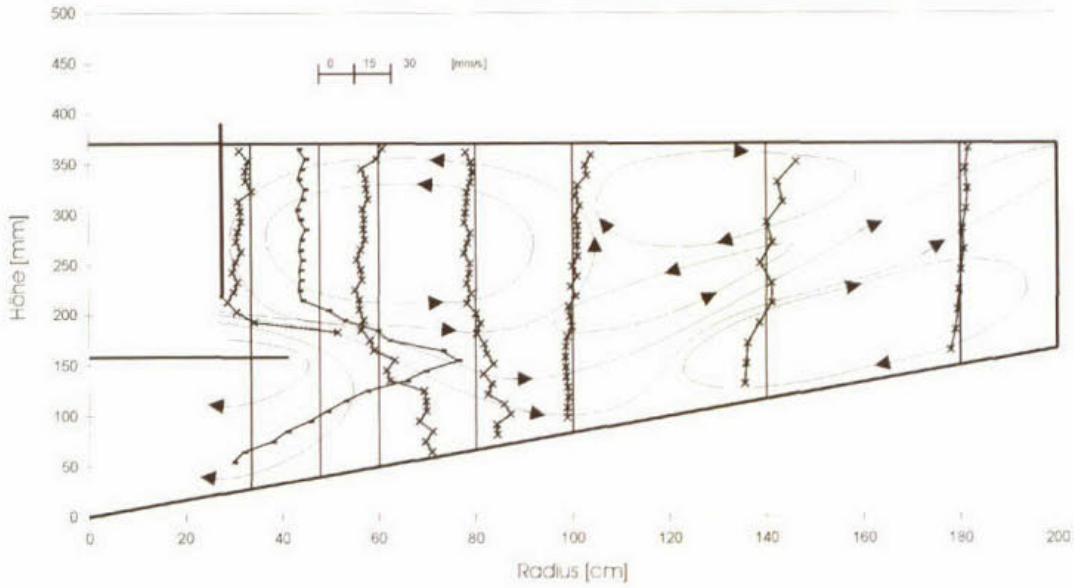

Fig. 5.3 *Velocity Profiles for Clear Water Case and guessed Streamlines*

First measurements with suspension showed for both cases with the deflection baffle mounted (S4 and D4) steady state situations with more or less reasonable heights for the layer of settled particles. Case S4 looked quite good with the height of the particles layer height up to the deflection baffle (Fig. 5.4), case D4 showed for some reason a higher particle layer although the load was less (Fig. 5.5). Nevertheless the system seemed to work. The problem with the filling of the tank did not occur anymore in these cases; the measures taken to overcome the problems worked apparently as was expected from the initial test runs.

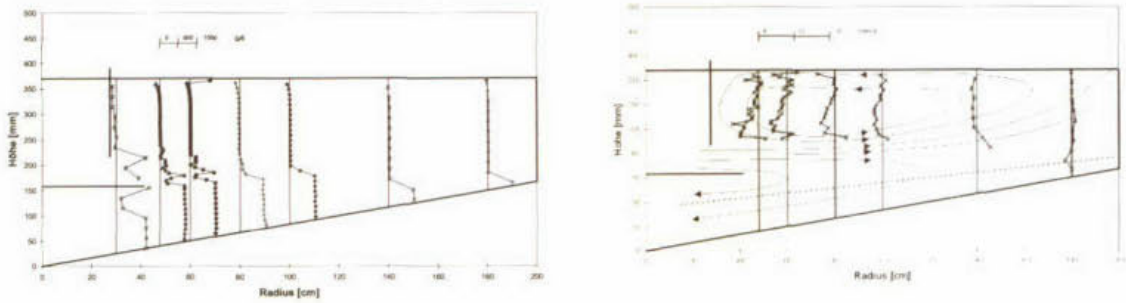

a) Concentration Profiles for Case S4

b) Velocity Profiles for Case S4 and guessed Streamlines

Fig. 5.4 *Measurement Case S4* ***with*** *Deflection Baffle*

After dismantling the horizontal deflection baffle the situation changed dramatically. Again it became clear that the settled particles had no tendency to move anymore but were only pushed around in circles by the scrapers as a quasi rigid body. The bottom layer with higher concentrations stopped flowing towards the hopper and a short-circuit flow of the suspension with inlet concentrations established from the inlet to the recirculation hopper. The lower inlet concentrations for the steady state situation of cases S5 (Fig. 5.6) and D5 (Fig. 5.7) in Tab. 5.1 are a consequence of this behaviour since finally more and more particles were stored in the settling tank instead of being returned to the mixing tank. So finally this revised system also failed due to insufficient moving ability of the settled particles.

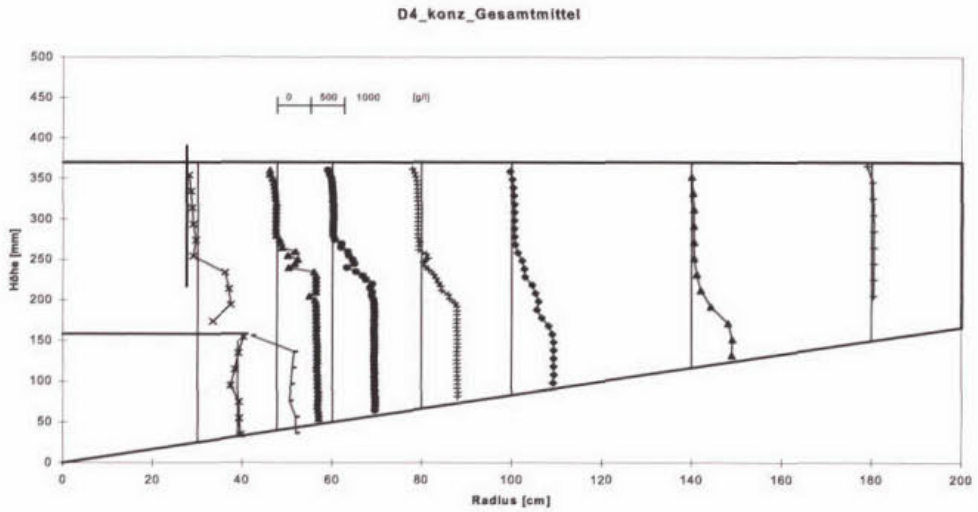

Fig. 5.5 *Measurement Case D4* ***with*** *Deflection Baffle. Concentration Profiles*

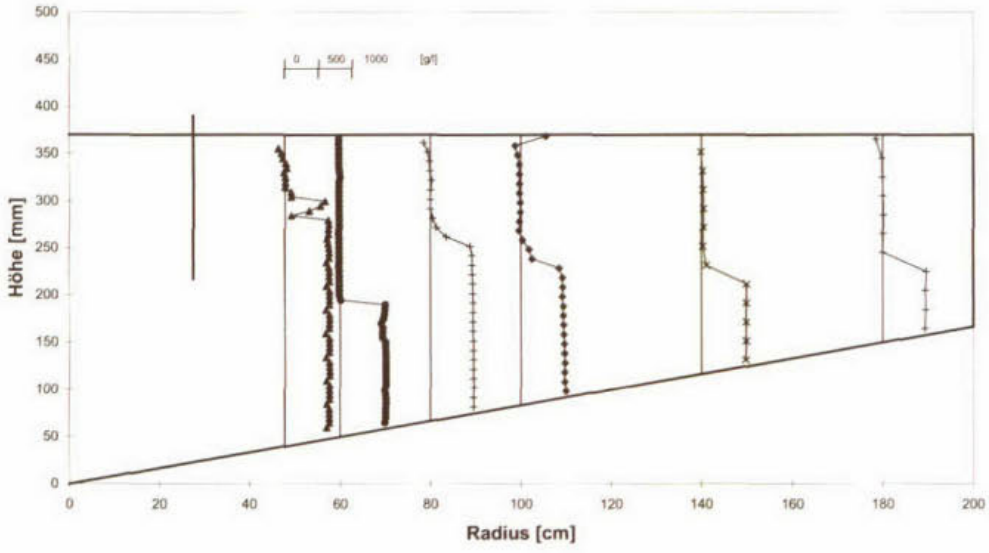

Fig. 5.6 *Measurement Case S5* ***without*** *Deflection Baffle. Concentration Profiles. Profile at R = 60 cm was measured before the System was in an Equilibrium i.e. before a Steady State Situation was reached*

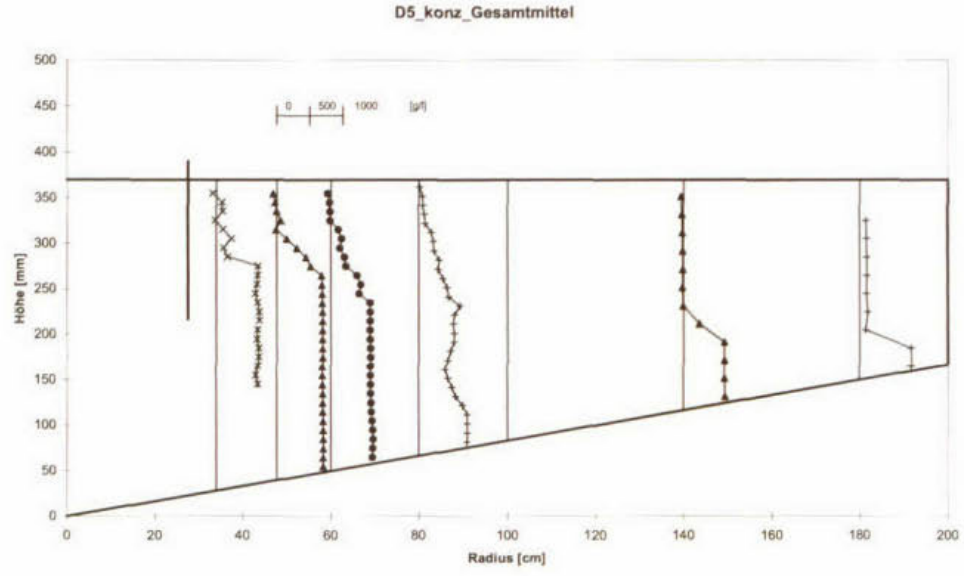

Fig. 5.7 *Measurement Case D5* ***without*** *Deflection Baffle. Concentration Profiles. The Particle Layer again reaches the Water Surface at Radius R = 1 m. Consequently the Inlet is totally blocked with suspension*

6 Test with Iron Hydroxide in the Suspension

A last – and finally also unsuccessful – test and general modification to the model as a full circular tank for steady state measurements was carried out which did not focus on the geometry, shape or technique of the model but on the flow behaviour of the settling material itself. The idea was to mix the Lewatit particles with iron hydroxide flocks and polymers to reduce the internal friction as well as the bottom friction by changing the properties of the suspension. With respect to this measure two reconstructions of the model were needed:

- a major increase of the side water depth (from 20 to 40 cm) leading to an increased detention time which allows the suspensions to produce flocks
- a polymer dosage device (Fig. 6.1)

As mentioned, the pure Lewatit particles did not fulfil the assumed flow properties in practice but stuck to the bottom and filled up the tank until almost all particles in the system were stored in it with the consequence that the inlet concentration dropped almost to zero. Further examinations led to the opinion that this problem could be overcome by adding iron hydroxide flocks $Fe(OH)_3$ and anionic polymers ("Cytec Superfloc 1820" or "Praestol A 3040" resp.) to the suspension in order to reduce inter-particle friction.

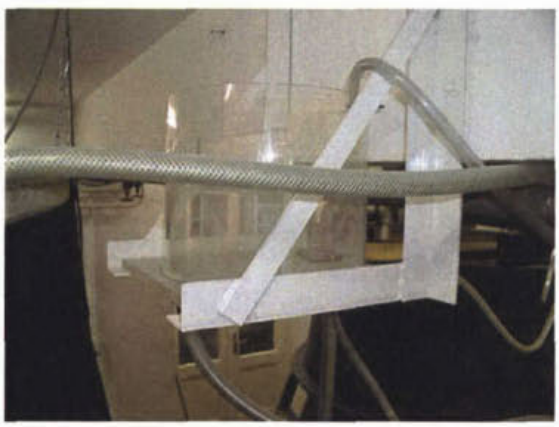

Fig. 6.1 *Dosing Device for Polymers*

Iron hydroxide was produced by mixing iron chloride with sodium hydroxide:

$$FeCl_3 \cdot 6H_2O + 3NaOH \rightarrow Fe(OH)_3 + 3NaCl + 6H_2O \qquad (6.1)$$

A major disadvantage of adding iron hydroxide was that for every mol $Fe(OH)_3$ three mol salt NaCl were added to the suspension (see eq. 3.1). To avoid density differences, this salt had to

be washed out by multiple dilution of the suspension with clear water. But dissolved salt does not only change the density of the suspension but also its conductivity. Since it was impossible to wash out all the salt a rest of salt was left in the suspension, which influenced the measuring with the concentration probe via the actual conductivity of the suspension.

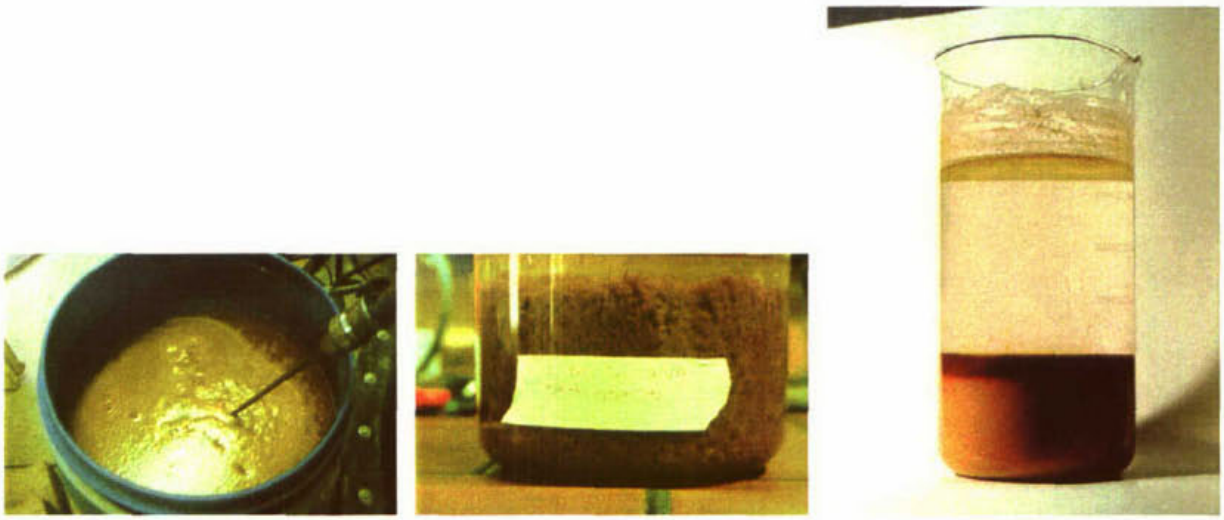

a) Mixing of Sodium Hydroxide and Iron Chloride to Iron Hydroxide

b) Flocks formed by Lewatit Particles plus Iron hydroxide plus polymers

c) Flocks destroyed by stirring. Iron hydroxide and Lewatit separated

d) Initial inflow situation with particles like in b)

e) After some hours of pumping flocks are non reversibly destroyed

f) Flow tests with particles like in c)

Fig. 6.2 *Model Sludge: Lewatit particles plus iron hydroxide and polymers*

Although first tests in vessels and small models looked promising, the new mixture did not keep its flow properties but flocks were destroyed irreversibly and the sludge bed again started to stick to the bottom (Fig. 6.3). The Lewatit particles settled out much faster than the flocks and so finally a film of iron hydroxide could be observed over a layer of Lewatit.

Fig. 6.3 *Also with Iron Hydroxide the System fails due to separation of Lewatit and Flocks.*

7 Final Measurements

7.1 ¾ Tank for Unsteady Starting Phase

After all the tests failed to overcome the problems in running a steady state model, it was decided to stop these efforts and to focus on a different flow problem: the unsteady starting phase of the filling process of the tank.

The idea is to learn about

- unsteady flow situations with
- gravity effects and
- settling of particles

and to compare these phenomena with their predictions by CFD computations – i.e. the main challenge for the numeric simulation for which the following equations for the momentum transport

$$\underbrace{\frac{\partial U_i}{\partial t}}_{\substack{\text{temporal}\\ \text{acceleration}}} + \underbrace{U_i \frac{\partial U_j}{\partial x_j}}_{\substack{\text{local}\\ \text{acceleration}}} = \underbrace{-\frac{1}{\rho}\frac{\partial p}{\partial x_i}}_{\substack{\text{deceleration}\\ \text{in positive}\\ \text{direction of pressure}}} + \underbrace{\frac{\partial}{\partial x_j}\left[\frac{\mu}{\rho} \cdot \left(\frac{\partial U_i}{\partial x_j} + \frac{\partial U_j}{\partial x_i} - \tau_{ij}\right)\right]}_{\text{Viscose Transport of Momentum}} + \underbrace{g\delta_{1j}\frac{(\rho - \rho_w)}{\rho_w}}_{\text{Buoyancy}} \qquad (7.1)$$

and the mass transport respectively

$$\underbrace{\frac{\partial X}{\partial t}}_{\substack{\text{temporal change}\\ \text{of Concentration}}} + \underbrace{X\frac{\partial U_j}{\partial x_j}}_{\substack{\text{convective change}\\ \text{of Concentration}}} + \underbrace{X\frac{\partial v_s}{\partial x_j}}_{\substack{\text{Convection}\\ \text{due to Setling}}} = \underbrace{\frac{\partial}{\partial x_j}\left(-\overline{u'_j\, c'}\right)}_{\text{(turbulent) Diffusion}} \qquad (7.2)$$

are used.

To determine the effects of the unsteady situation the first term of the momentum transport equation – the temporal acceleration – has to be predicted correctly. The gravity effect leading to the physical phenomena that the inflowing jet is – due to its higher density with respect to the ambient fluid – accelerated downwards, is represented by the right hand side term for buoyancy. This term is the second very sensitive part of the numerical simulation. The convection due to settling, represented by the last term on the left hand side of the mass

transport equation, is a third critical parameter responsible for success or failure of computations for settling tanks.

All these three phenomena can be observed in the filling phase of the tank.

a) Quarter Sector taken out of the Flow Regime

b) Detail of the Inlet (View from quarter sector)

c) Tubes attached to allow Sucking off of Suspension

d) Photo and Video Camera

e) Detail of the Inlet covering ¾ of the Tank

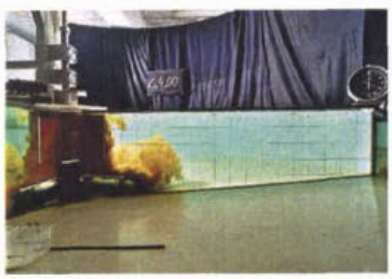

f) Initial Situation of Unsteady experiment

Fig. 7.1 *Set-Up of Model for Unsteady Experiments*

For these experiments however neither the concentration probe nor the velocity probes could be used since both systems need a data sampling time of approx. 20 to 60 seconds to gain reasonable mean values of the measured quantities whereas the unsteady experiments last only 60 to 90 seconds. So other methods had to be used to quantify the unsteady flow behaviour.

- Flow visualization movies and photos were taken from which the propagation speed of the front of the density current could be determined. (Fig. 7.1 d). Although the ADV probe was used additionally, it became clear during the experiments that this probe would not deliver useful results since it was not provided with a sufficient amount of particles in the measurement volume. So the analysis of velocities finally focused on the picture series.
- Concentrations were measured by sucking off suspension near the bottom and weighing the dried portion of particles in the sample (Fig. 7.1 c,). The first idea was to

take samples at different heights above the bottom. But the turbidity, which could be observed in the tank did not really show the flow of higher concentrated suspensions but fractions of separated iron hydroxide in very low concentrations of some one to five percent of the total inlet concentration. Only directly above the bottom it was finally possible to measure concentrations near to inlet concentrations which is mainly determined by the fraction of Lewatit rather than by iron hydroxide.

For these investigations the model had again to be changed. The scraper devices were dismantled and a 90° sector was taken out of the flow regime (Fig. 7.1 a,b) separating it with transparent walls. In this sector a photo as well as a video camera was placed facing horizontally to the right hand wall (Fig. 7.1 d). Holes in the left hand wall carrying small tubes were placed at radial positions R =80 cm, R =120 cm and R =120 cm to allow sucking off of suspension near the bottom. This was finally done at three radii with four small plastic containers at each radius. During the measurements the containers were filled with suspension sucked off at different measurement points by small tubes leaving the ¾ tank through holes in its side wall. For four times every twenty seconds the three actually filled containers were replaced by the next three empty containers. So four samples over a total of 80 seconds could be sucked off. After drying and weighing of these samples the concentration could be determined as a function of location and time. All measurements were carried out with a horizontal deflection baffle at the inlet.

7.2 Test Cases

Measurements were carried out for the following test cases:

	C_0 [g/l]	q_A [m/h]	R [-]
A_1, A_2	200	0.45	1.1
B_1, B_2, B_3	200	1.0	0.45
C_1, C_2	90	0.5	0.8
D_1, D_2	200	2.0	-

Tab. 7.1 *Test Cases for Unsteady Measurements in ¾ Tank*

Or, more detailed:

Experiment Date:		Radius	Position	C_0 [g/l]	Q_{In} [l/s]	Q_{Rec} [l/s]	Q_{Out} [l/s]	PE [ml/s] 0.33% dilution	q_A [m/h]	Rec. Fac. R [-]	v_{In} [cm/s]	$Fr_{D,In}$	H_{In} [cm]	Remarks
16.12.1999	A_1	700	583	207	2.5	1.1	1.4	7	0.42	1.27	1.30	0.0565	11.1	• $v_0 = 0$ • concentration measurements not available • concentration probes ≈ 4cm above ground
05.01.2000	A_2	700	633	204	2.5	1.3	1.2	5	0.46	1.08	1.30	0.0570	11.1	• $v_0 \neq 0$ • concentration probes ≈ 4cm above ground
07.01.2000	B_1	700	573	196	3.9	1.3	2.6	5	0.99	0.50	2.03	0.0905	11.1	• $v_0 \neq 0$ • concentration probes ≈ 4cm above ground
21.02.2000	B_2	700	573	193	3.9	1.2	2.8	5	1.07	0.39	2.03	0.0913	11.1	• $v_0 \neq 0$ • concentration probes ≈ 4cm above ground
06.04.2000	B_3	700	573	196	3.9	1.3	2.7	5	1.03	0.48	2.09	0.0929	11.1	• $v_0 \neq 0$ • concentration probes ≈ 1cm above ground • C_{In}(t=183 s)
13.01.2000	C_1	700	573	90	2.5	1.2	1.3	3	0.53	0.79	1.30	0.0859	11.1	• $v_0 \neq 0$ • concentration probes ≈ 4cm above ground
28.01.2000	C_2	700	573	90	2.5	1.1	1.4	3	0.53	0.79	1.30	0.0858	11.1	• $v_0 \neq 0$ • concentration probes ≈ 4cm above ground
04.05.2000	D_1	700	573	195	4.7	0.0	4.7	10	1.80	-	2.45	0.1095	11.1	• $v_0 = 0$ • concentration probes ≈ 1cm above ground • C_{In}(t=32 s) & C_{In}(t=156 s) • Q_{In} (pump at 50 Hz) ⇒ estimated from weir outflow
02.06.2000	D_2	700	573	191	5.7	0.0	5.7	10	2.18	-	2.97	0.1342	11.1	• $v_0 = 0$ • concentration probes at ground level • C_{In}(t=49 s) & C_{In}(t=154 s) • Q_{In} (pump at 50 Hz) ⇒ estimated from weir outflow

7.3 Analysis of the Measurements

7.3.1 Concentration Measurements

As was mentioned already, the first concentration measurements not very close to the bottom of the tank resulted in very low concentrations although the turbidity was not recognizably smaller than at other points in the suspension. This was a consequence of the separation of turbid but light iron hydroxide suspension from the more dense Lewatit particles. Only measurements directly above the bottom showed concentrations of the order of fifty percent of the inlet concentration but also never reached values close to or higher than the inlet concentration. Such high concentrations however should be expected near the bottom due to settling and thickening processes and were obtained in the calculations presented in 7.4.

As a consequence these improved measurements could not really be trusted. As an example, the evolution of the measured concentrations for case B_3 are presented in the following figures (Fig. 7.2 to Fig. 7.5). As can be seen, the concentrations never came even near the inlet concentration and certainly did not rise above it. Only a maximum of approx. 35 % C_{in} was reached during this measurement:

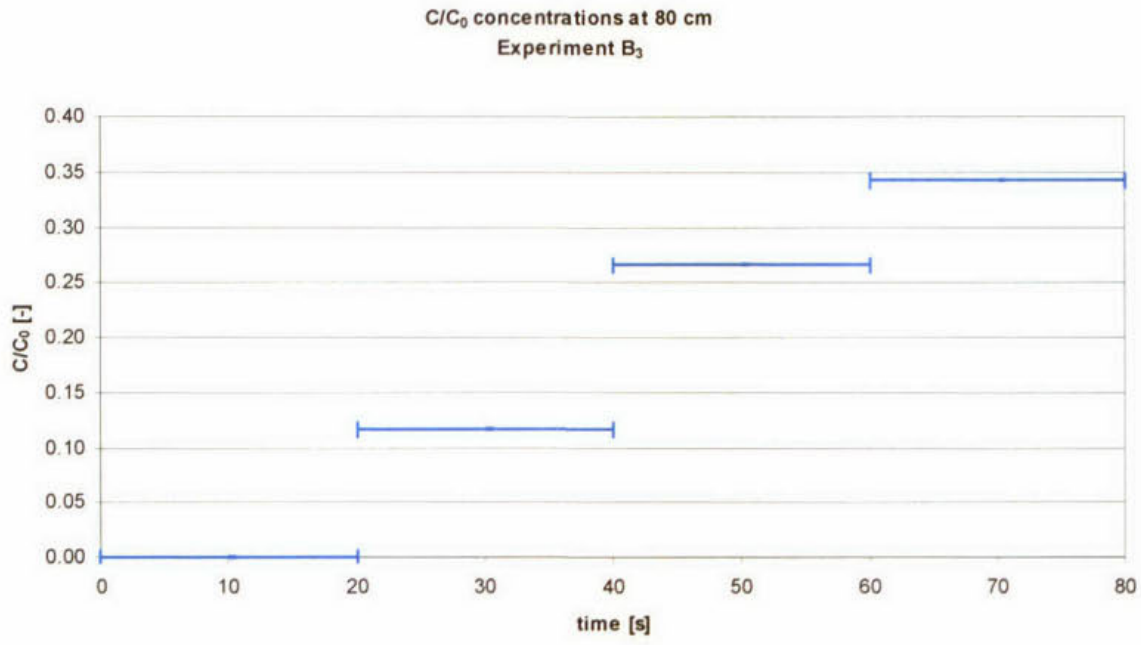

Fig. 7.2 *Evolution of Measured Concentrations at Radius R = 80 cm for Case B_3*

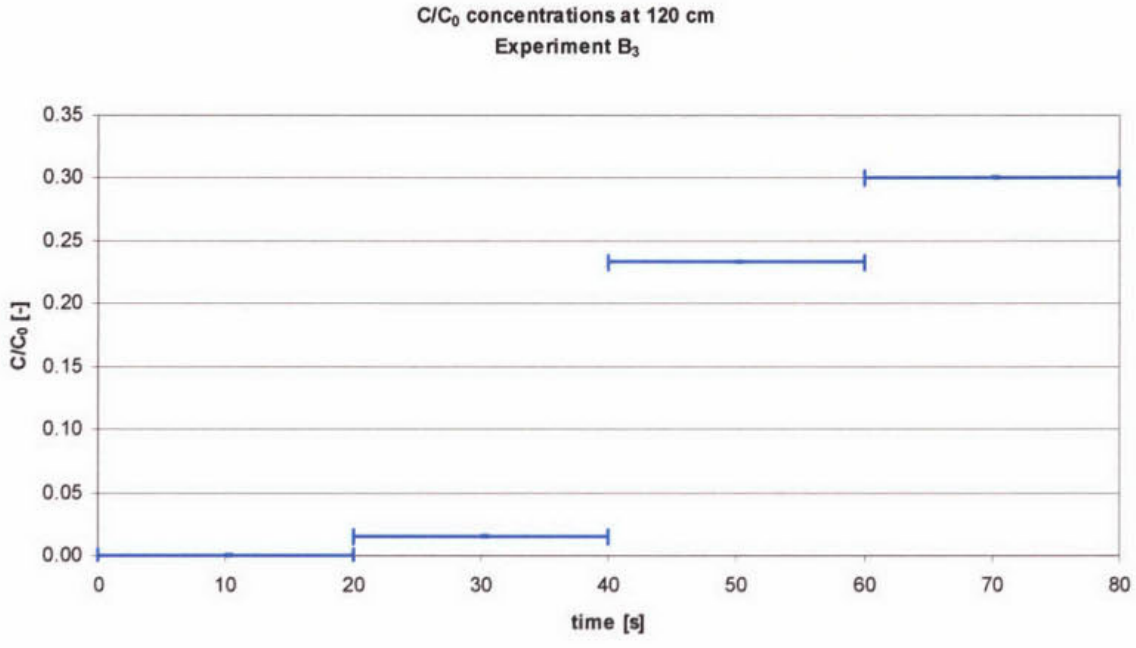

Fig. 7.3 *Evolution of Measured Concentrations at Radius R = 120 cm for Case B_3*

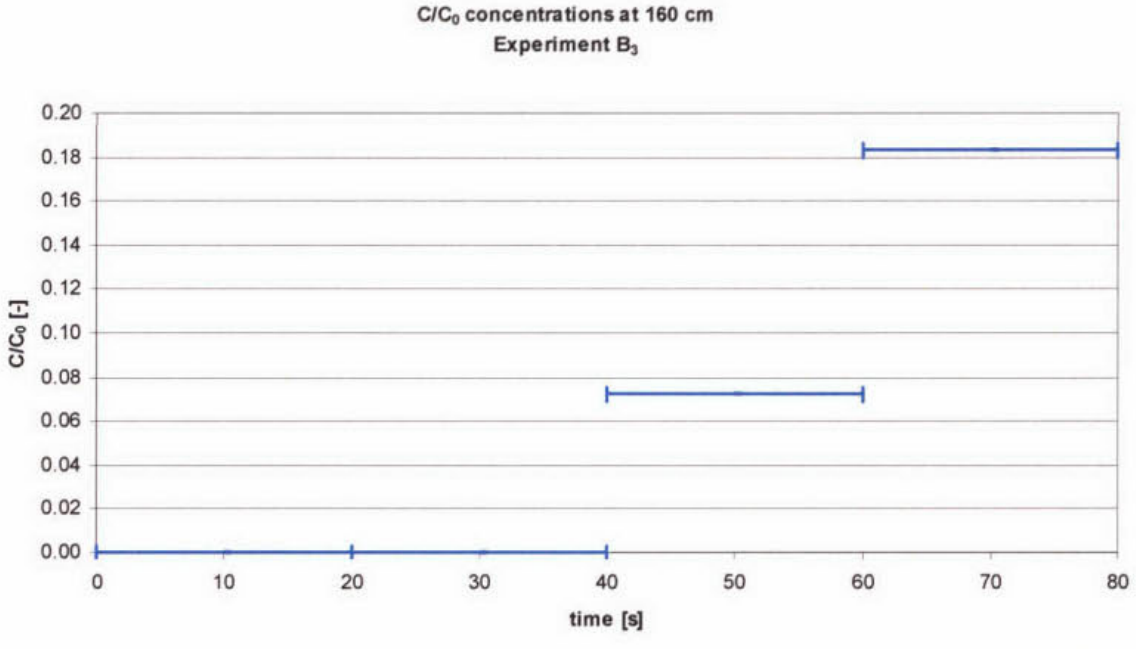

Fig. 7.4 *Evolution of Measured Concentrations at Radius R = 160 cm for Case B_3*

Combined into one diagram, the concentration measurements for case B_3 result in Fig. 7.5, which shows development with time of the concentration at the three radial measurement positions. Because of the low trustworthiness of the concentration measurements, results for the other measurements are not included here.

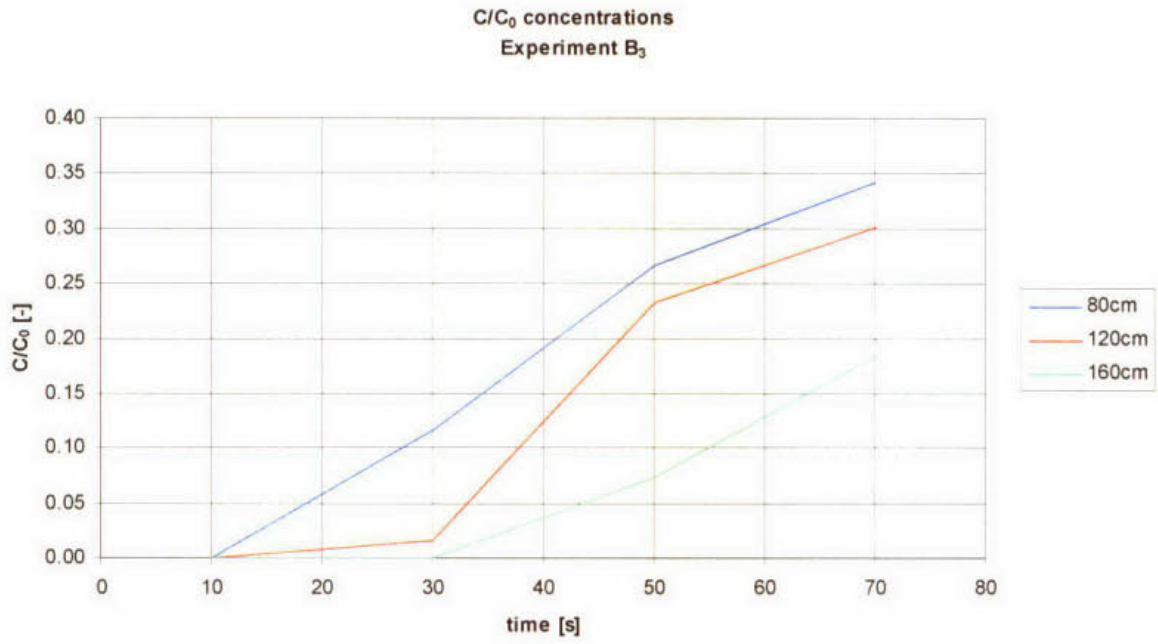

Fig. 7.5 *Evolution of Measured Concentrations at all three Radii for Case B_3. Maximum Concentration never exceeds 35 % of the inlet Concentration*

7.3.2 Suspension Front Spread

The photo series (see parts a) of Fig. 7.12 – Fig. 7.15) turned out to be the best and only reliable source for analysis of the experiments in the ¾ tank. The position of the suspension front determined from these photographs and the video recordings is given in Fig. 7.6 to Fig. 7.9 for all the measurements of the four test cases. Two points are to be mentioned on these optical suspension front observations, which restrict somewhat the meaningfulness of these results. First, the turbidity, which is observed, represents once more the non-settleable part of the suspension rather than the density current of the flow. At least at the front, however the velocity of the turbidity should be determined mainly by the density current, which means in other words that the turbidity front, which is examined here, also represents the density front. Secondly the flow properties of the settled particle layer were again such that they stuck to the bottom rather than flowing towards the sludge hopper once the suspension had thickened. This is opposite to the behaviour expected to occur in real tanks that underlies the numerical simulations which will be shown in chapter 7.4.

The examination of the photos yielded the following suspension front spread for the different cases:

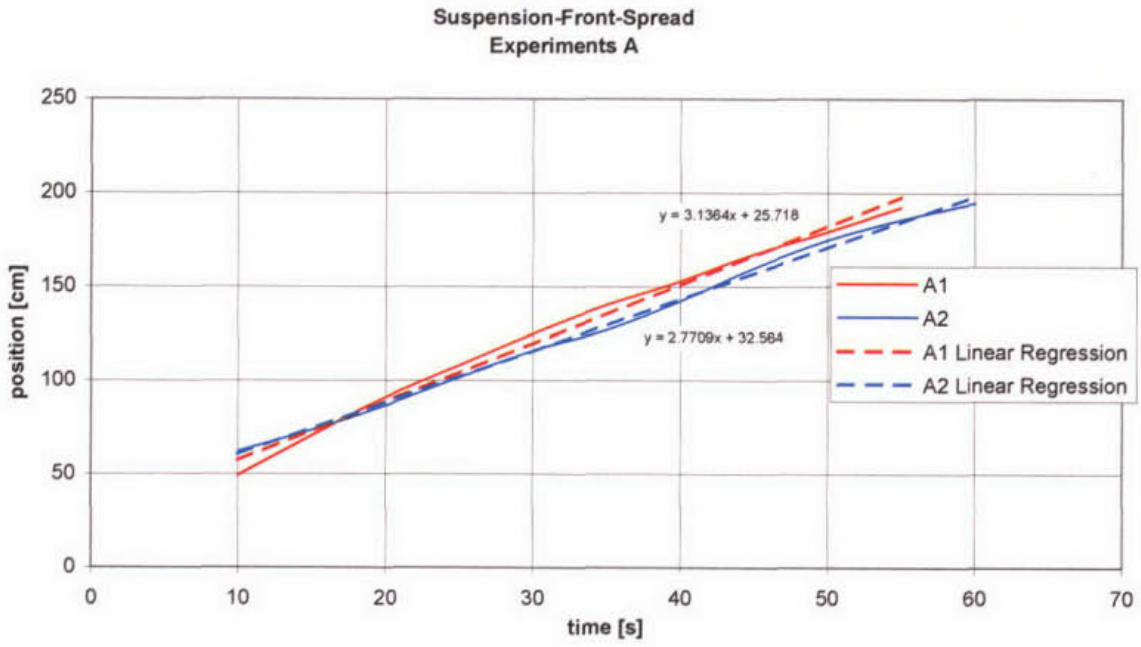

Fig. 7.6 *Spread of Suspension Fronts for Measurements fitting the A-Case and Linear Regressions to these Lines of Spread*

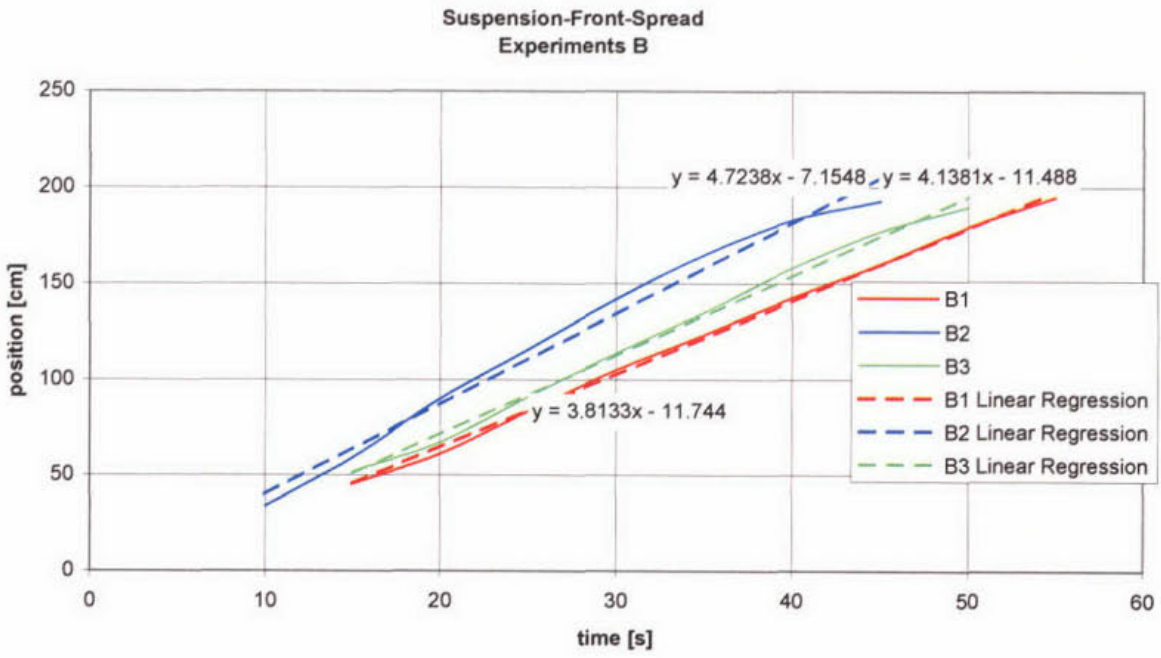

Fig. 7.7 *Spread of Suspension Fronts for Measurements fitting the B-Case and Linear Regressions to these Lines of Spread*

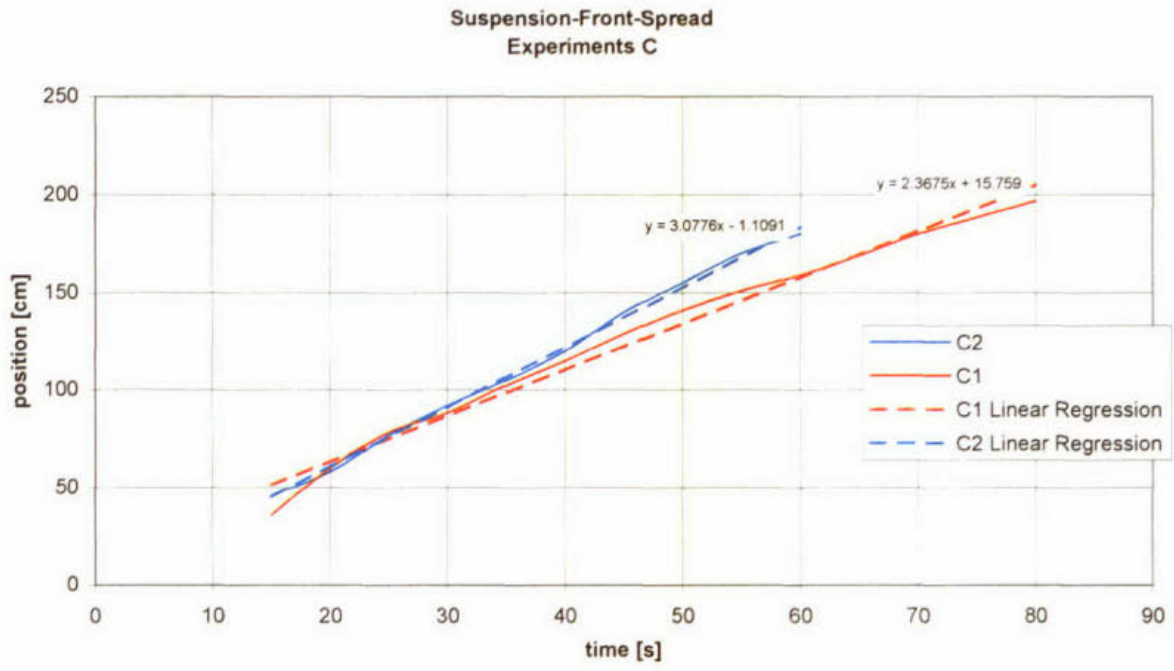

Fig. 7.8 *Spread of Suspension Fronts for Measurements fitting the C-Case and Linear Regressions to these Lines of Spread*

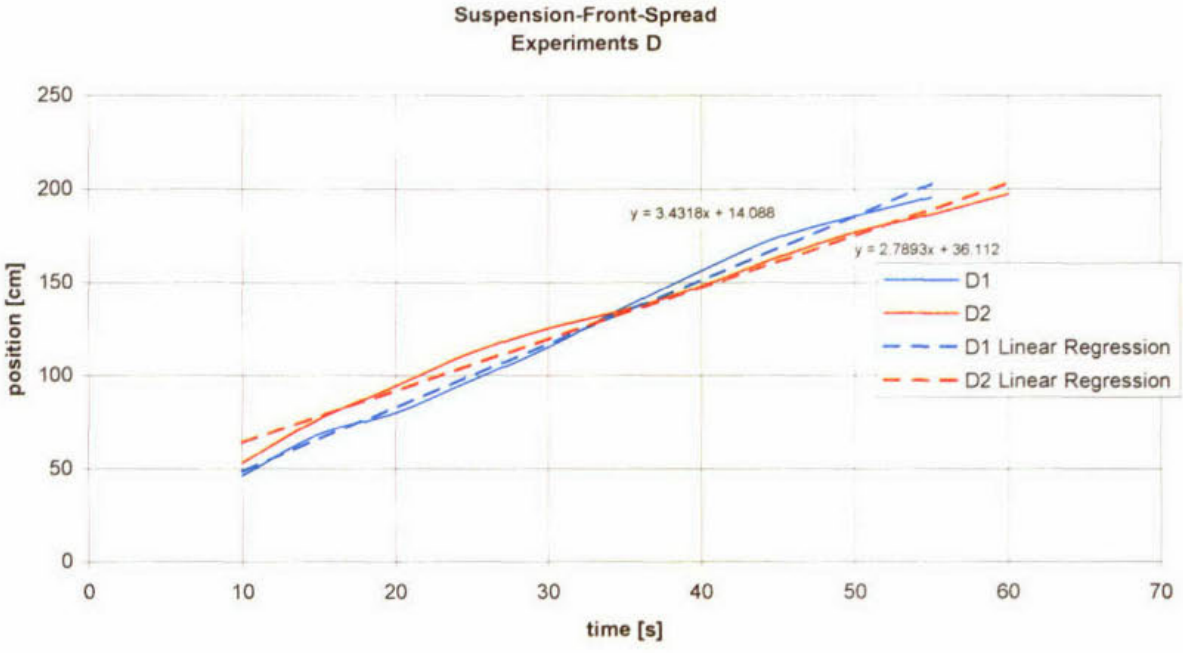

Fig. 7.9 *Spread of Suspension Fronts for Measurements fitting the D-Case and Linear Regressions to these Lines of Spread*

Bringing the linear interpolations from one representative measurement of each case

		A_1			B_3			C_2			D_2	
Time t [s]		Position [cm]	y=3,1364x+25,718		Position [cm]	y=4,1381x-11,488		Position [cm]	y=3,0776x-1,1091		Position [cm]	y=2,7893x+36,112
0		0			0			0			0	
5		0	41.4		0	9.2025		0	14.2789		0	50.0585
10		49	57.082		0	29.893		0	29.6669		53.3	64.005
15		70.5	72.764		52	50.5835		46	45.0549		76.6	77.9515
20		91	88.446		67	71.274		58	60.4429		94.6	91.898
25		108	104.128		91	91.9645		77	75.8309		112.5	105.8445
30		125	119.81		114	112.655		92	91.2189		125.4	119.791
35		140.5	135.492		135	133.3455		105	106.6069		135.3	133.7375
40		153	151.174		158	154.036		120	121.9949		148.3	147.684
45		167.5	166.856		177	174.7265		140	137.3829		163.9	161.6305
50		179.5	182.538		190	195.417		155	152.7709		177.1	175.577
55		192.5	198.22					170	168.1589		186.7	189.5235
60								180	183.5469		197.4	203.47

into one diagram with lines through the origin leads to the following figure:

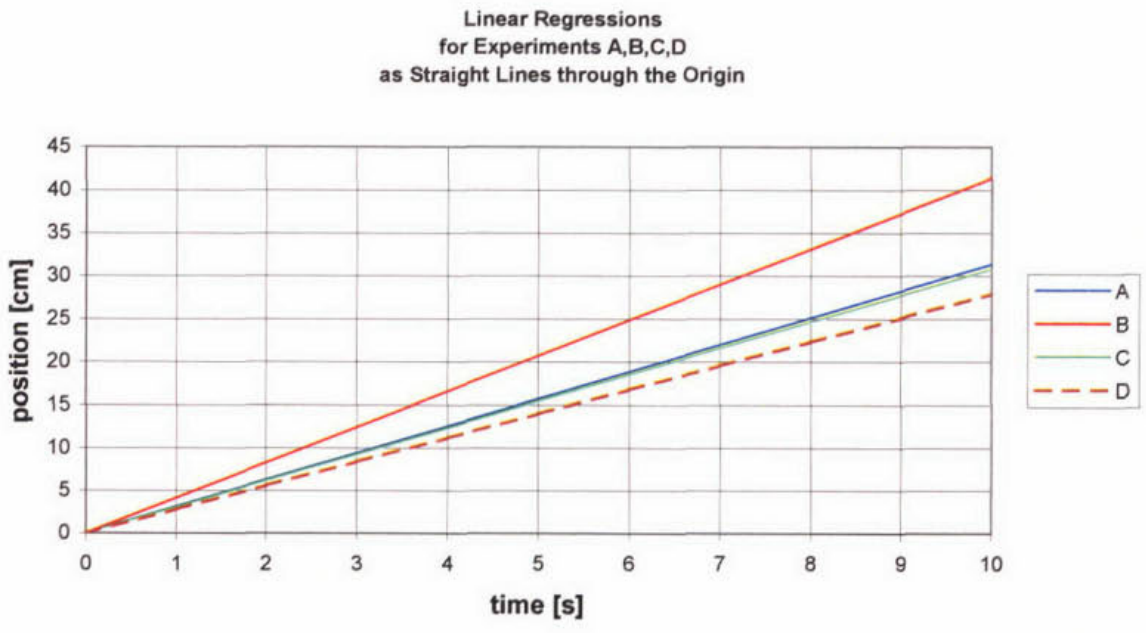

Fig. 7.10 *Linear Regressions for one Measurement of each Case*

Influence of Buoyancy on Spreading Speed

Generally the time for the spread of the front of a density current i.e. its speed should be dependent on the Densimetric Froude number. For this reason it seemed to be useful to plot the front velocity against the Densimetric Froude numbers of the different measurements (Fig. 7.11). This figure however shows no clear trend. Obviously there are more dependencies for the velocity of the front in these measurements. The dependency on parameters like the recirculation was not further investigated within the framework of this research.

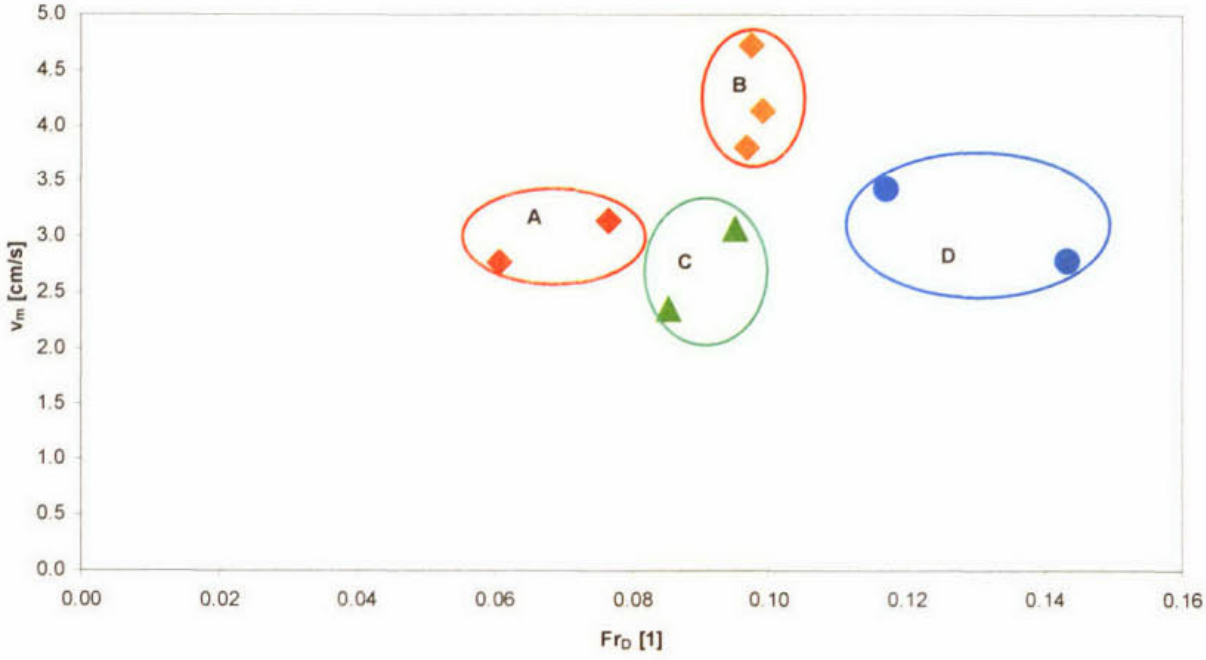

Fig. 7.11 *Velocity of the Front plotted against the Densimetric Froude Number Fr_D, derived with the velocity and the density of the inlet jet*

7.4 Comparison with Computations

The four experimentally studied test cases (parameters see Tab. 7.1) were also simulated with the numerical model developed at the Institute for Hydromechanics. This model is described in detail in Lakehal et al (1999) but a later version was used which ensures mass conservation. Also, instead of the Takács relation for the settling velocity, the Mandersloot relation (2.1) based on own measurements was employed. The simulation is based on the numerical solution of the momentum and particle concentration equations (7.1) and (7.2) together with the continuity equation. The effects of turbulence are accounted for by the k-ε turbulence model. The calculations start with clear water at rest in the tank; at $t = 0$ the inflow of sediment-laden water is switched on at the upper left inflow boundary, corresponding to the flow rate and inflow concentration conditions given in Table 7.1. The unsteady flow and concentration field developing is then calculated with time steps of $\Delta t = 0.25$ s in the initial phase of tank filling for which visual observations have been made in the laboratory tank.

In parts a) of Fig. 7.12– Fig. 7.15 the flow visualisation pictures at various times after starting the suspension inflow are compared with calculations showing the regions in which the suspension concentration is larger than 1 g/l. Since the start of the flow in the experiment (initiated by opening valves) is not precisely known, the first suspension contour of the simulation is synchronised with the distribution of the first measurement picture. All following measurement pictures and suspension contours of the simulation are then given in time steps of $\Delta t = 10$ s. As can be seen, there is in all cases reasonably good agreement between calculated and measured position of the suspension front in the time before this front reaches the outer wall of the tank. The thickness of the suspension layer in calculation and visual observation cannot be compared directly because in the experiment the suspension separates into heavier Lewatit particles settling near the bottom and basically unsettlable iron hydroxide particles staying above the bottom layer, while in the calculations a monodisperse suspension was used.

In parts b) of Fig. 7.12– Fig. 7.15 the position of the density front at various times determined from the observations and the calculations is compared. Straight lines are drawn through the measurements points and the calculations allowing a direct comparison of the observed and

calculated front propagation speeds. It should be noted that in the figure parts b) the start of flow has not been synchronised between calculations and measurements so that there is a shift in effective starting time. Also, mainly calculation results below 40 seconds have been used for determining the propagation velocity (gradient of front positions), because beyond 40 seconds a phenomenon occurred in the calculations, which is not present in the experiments. This phenomenon can be seen from Fig. 7.16 – Fig. 7.17 showing the development of the flow and concentration field in the calculations only for case C. In the density current the particles settle and the concentration increases near the bottom, reaching values above the inlet concentration, which is to be expected also in real sedimentation tanks. When this happens, starting at around 40 seconds, a counter density current develops along the sloping bottom, i.e. a movement of the high concentration layer towards the sludge hopper. This opposes the outward flow from the discharge and where the two meet the outward flow separates from the bottom and is directed upward and a local recirculation region develops. This region, which can also be seen as a hump in the calculation pictures (parts a) of Fig. 7.12– Fig. 7.15 and Fig. 7.16) moves to the left and increases in height. In the extreme, the region looks as shown in Fig. 7.18 for case B. The counter density current and the circulation region over which the outward flow has to move, retard the movement of the primary density current and temporarily stop it completely. In the experiment this phenomenon does not occur because, again, when the particles settle on the ground, they stick there and do not move so that a counter density current does not develop and the primary current propagates without opposition. Hence, calculations and experiments should only be compared for times when the counter density current is absent, i.e. for times smaller than 40 seconds. Cases A and C are particularly affected by the described counter current phenomenon and here in fact the propagation of the primary current stopped due to this phenomenon before it reached the outer wall. However, during the initial time less than 40 seconds the propagation speed is quite well predicted. Better agreement should really not be expected in view of the assumption of monodisperse particles made in the calculations while in the experiments there is a separation between the heavier Lewatit and the lighter iron hydroxide particles.

On the whole, this can be said for all the test cases so that the model can be judged to predict the initial unsteady flow development fairly well.

7.4.1 Case B

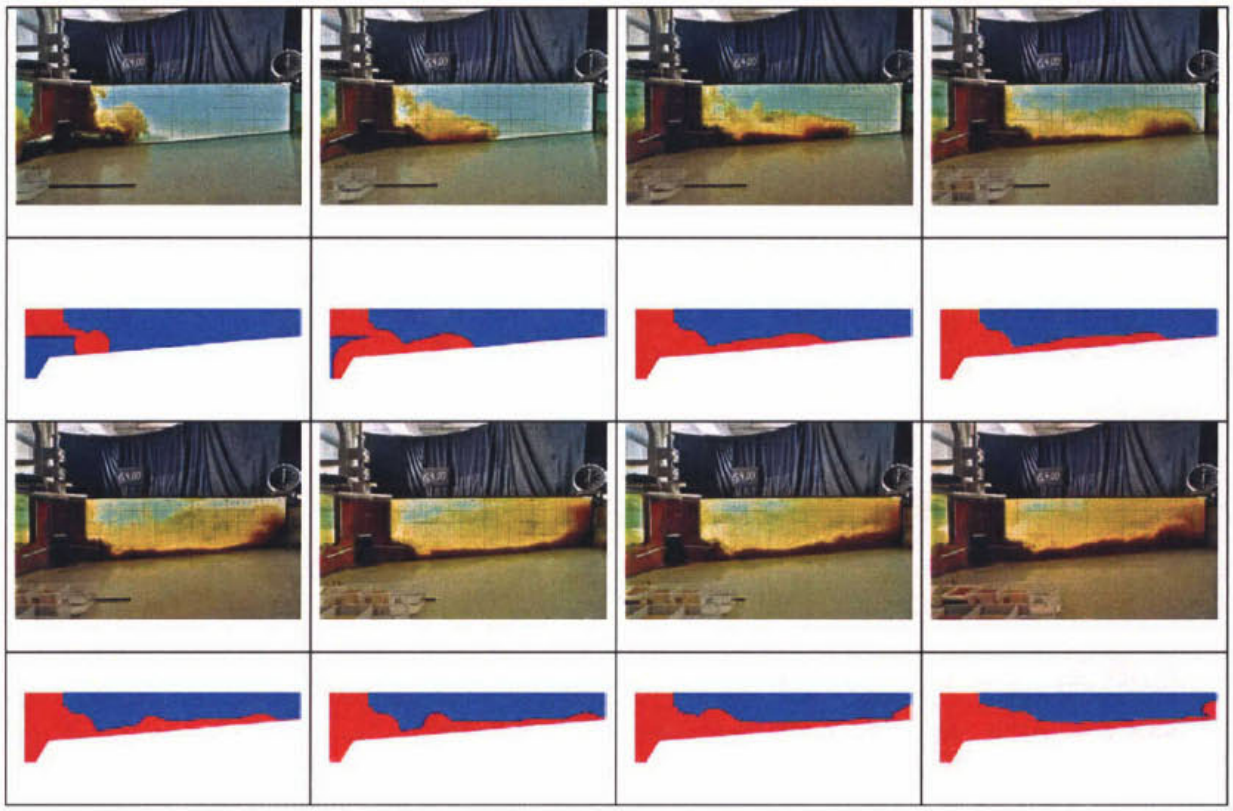

Fig. 7.12 a Series (time steps Δt = 10 s) of Measured versus Computed Suspension Front for Case B

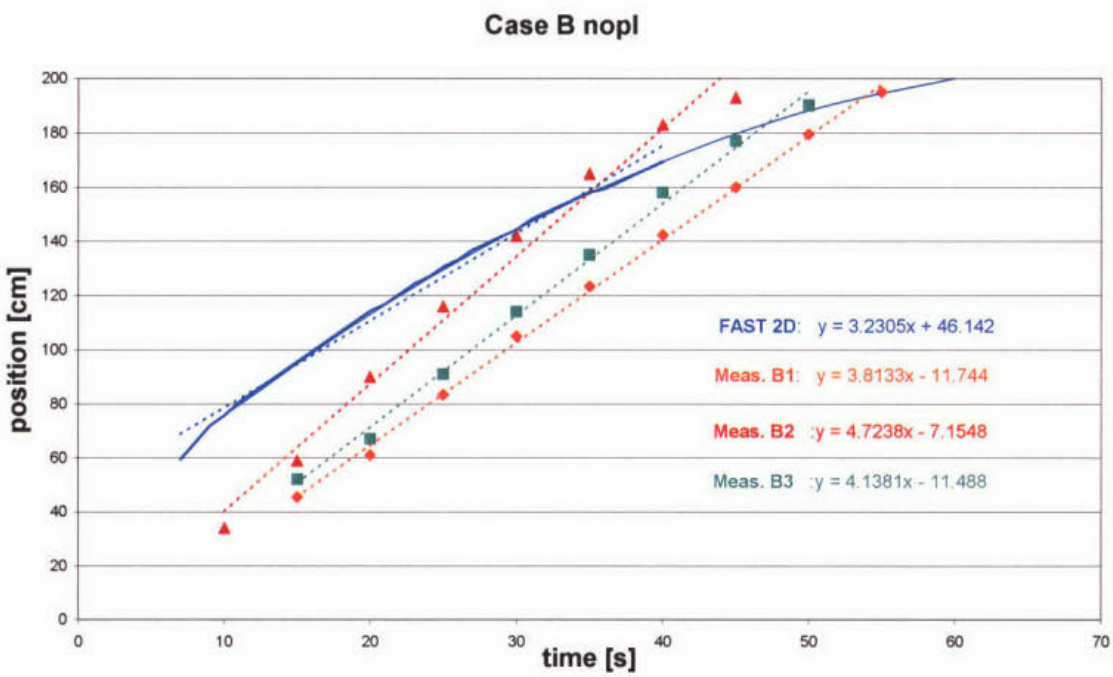

Fig. 7.12 b Spread of Suspension Fronts for Measurements (B-Case) and Computation

7.4.2 Case D

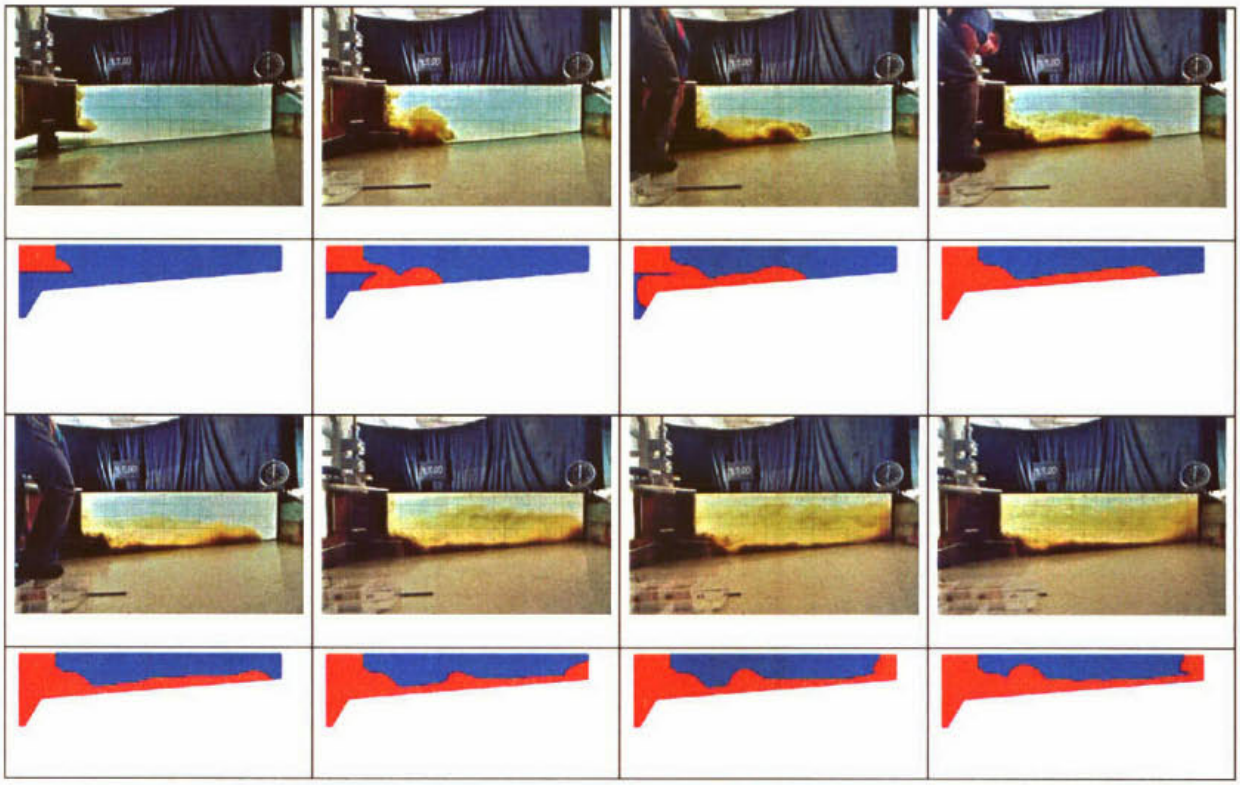

Fig. 7.13 a Series (time steps Δt = 10 s) of Measured versus Computed Suspension Front for Case D

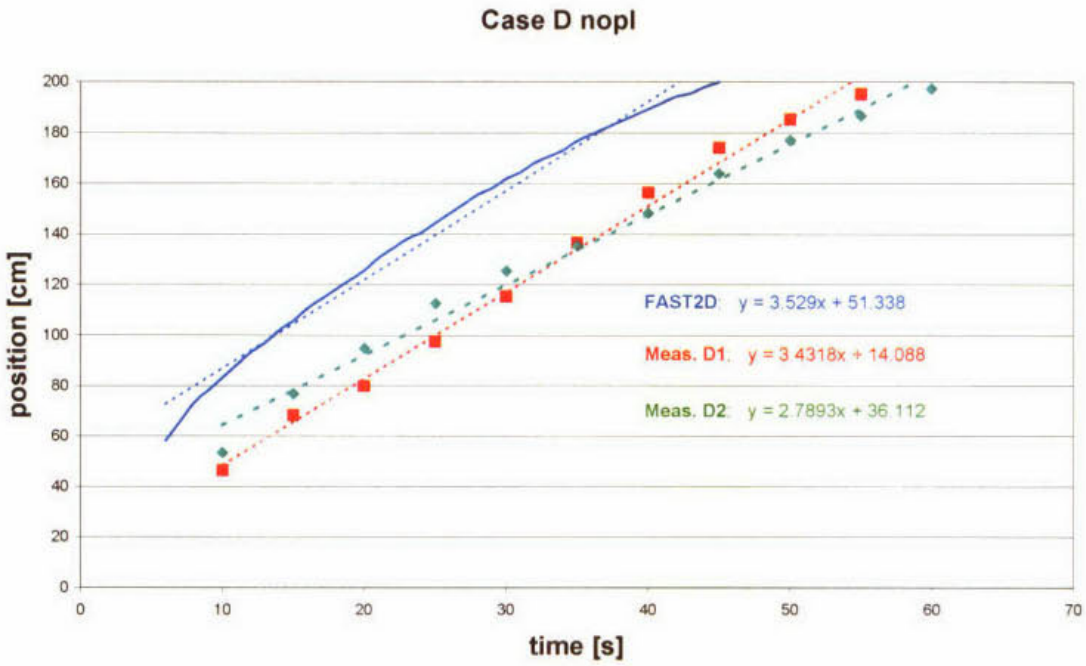

Fig. 7.13 b Spread of Suspension Fronts for Measurements (D-Case) and Computation

7.4.3 Case A

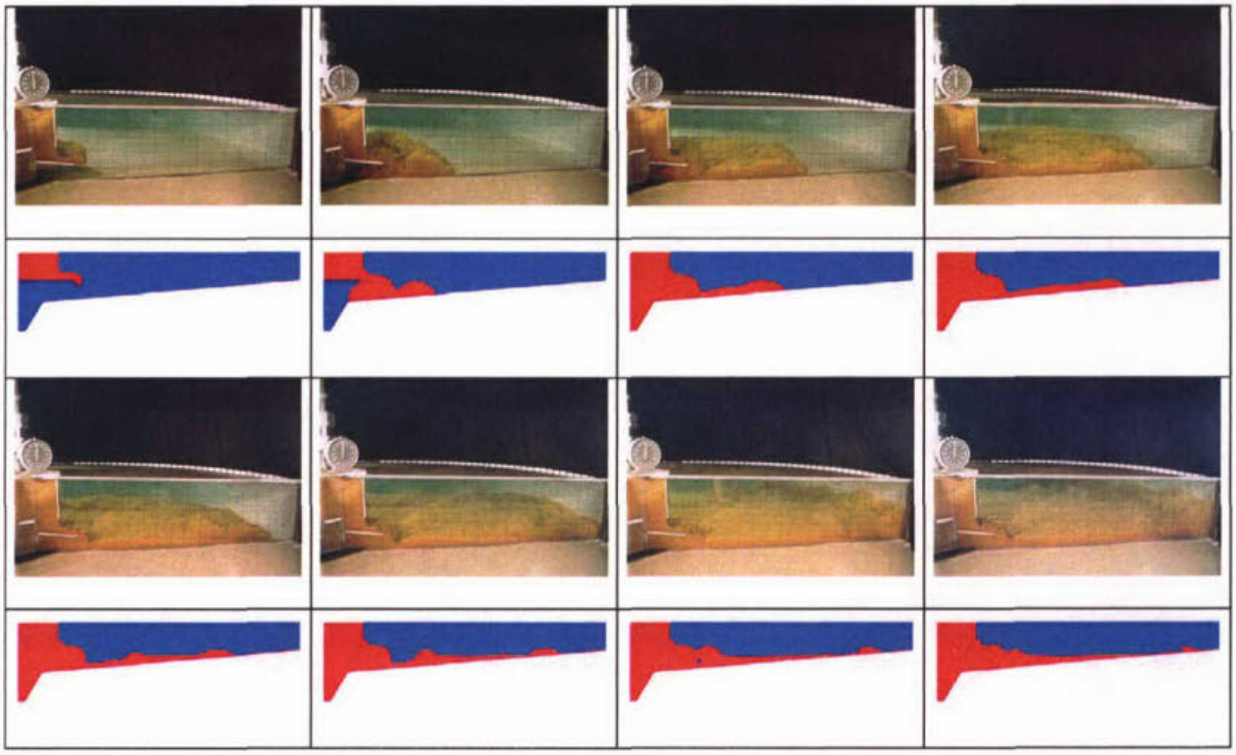

Fig. 7.14a Series (time steps Δt = 10 s) of Measured versus Computed Suspension Front for Case A

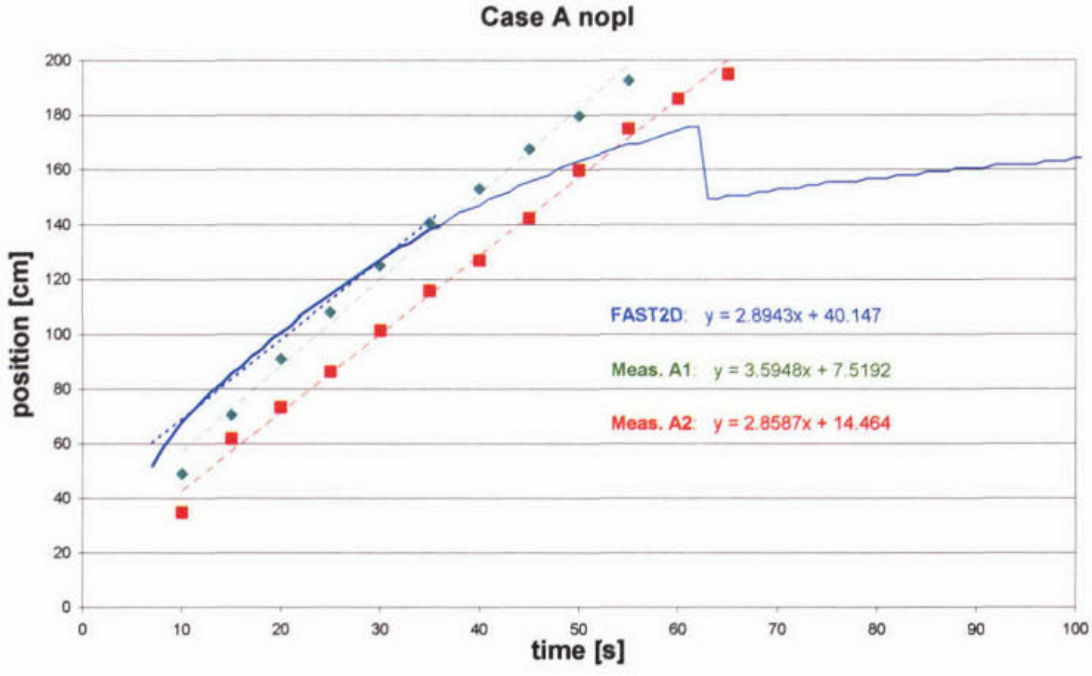

Fig. 7.14b Spread of Suspension Fronts for Measurements (A-Case) and Computation

7.4.4 Case C

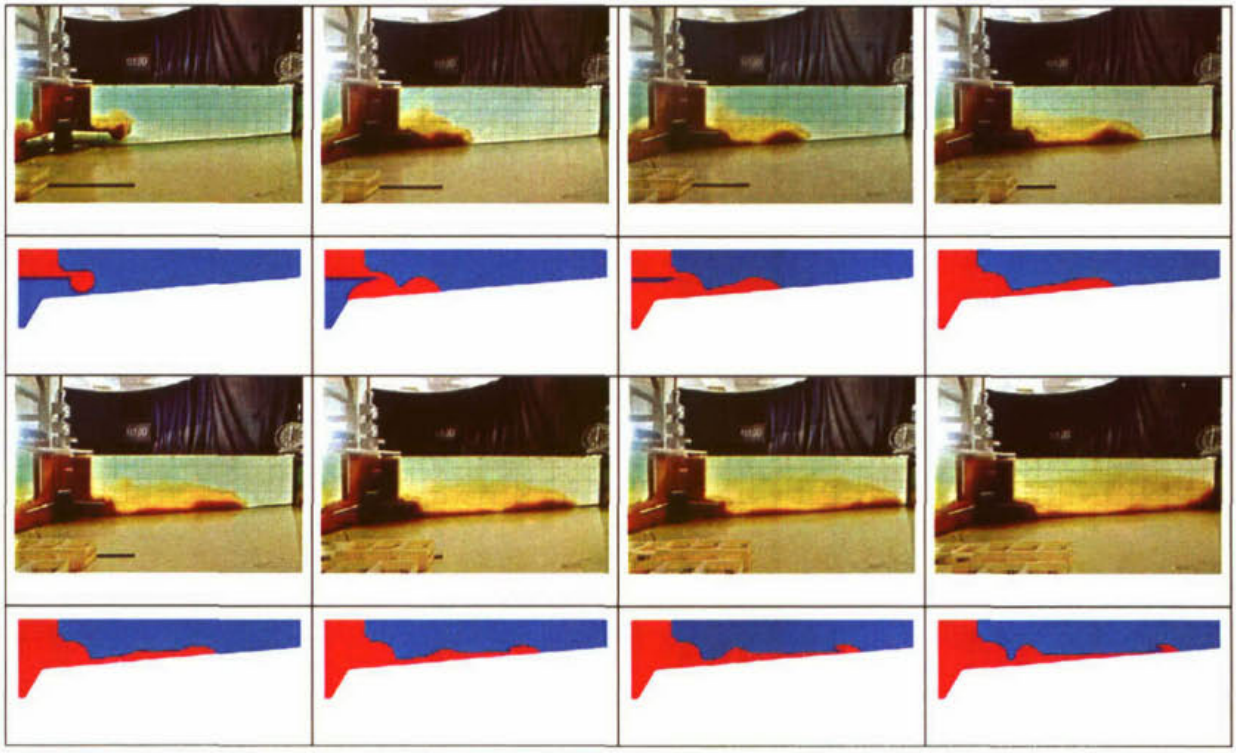

Fig. 7.15a Series (time steps Δt = 10 s) of Measured versus Computed Suspension Front for Case C

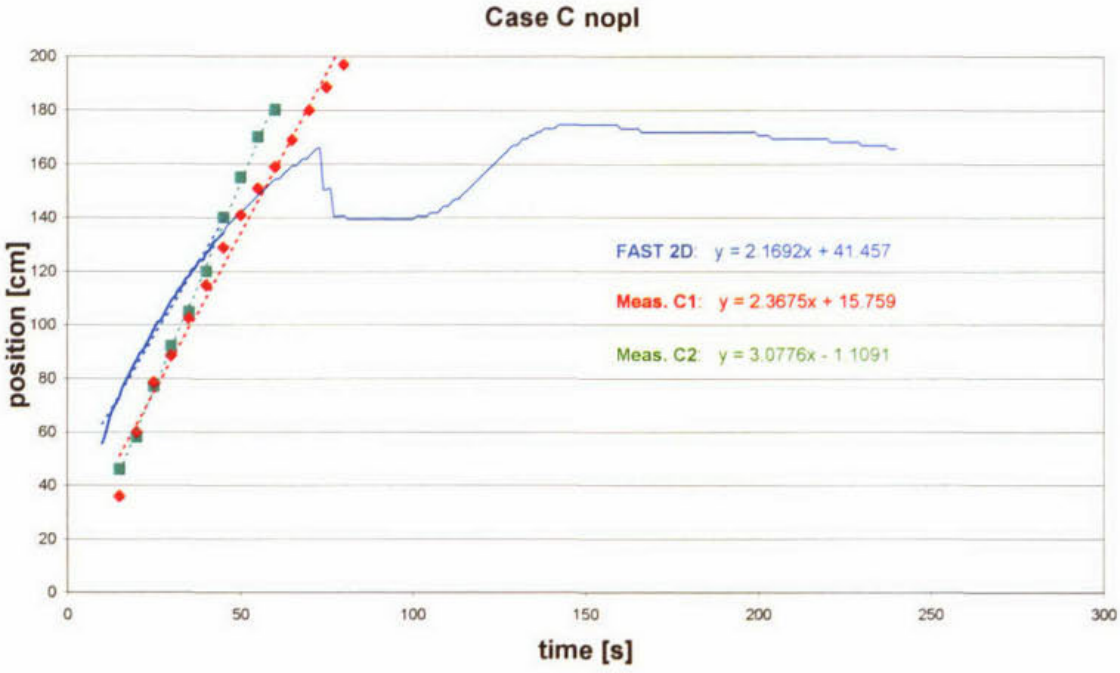

Fig. 7.15b Spread of Suspension Fronts for Measurements (C-Case) and Computation

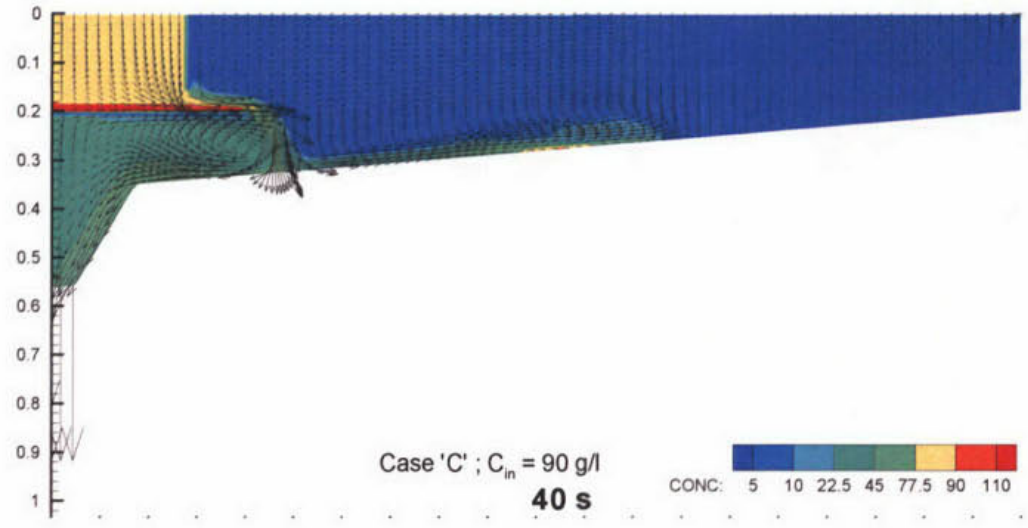

Fig. 7.16a

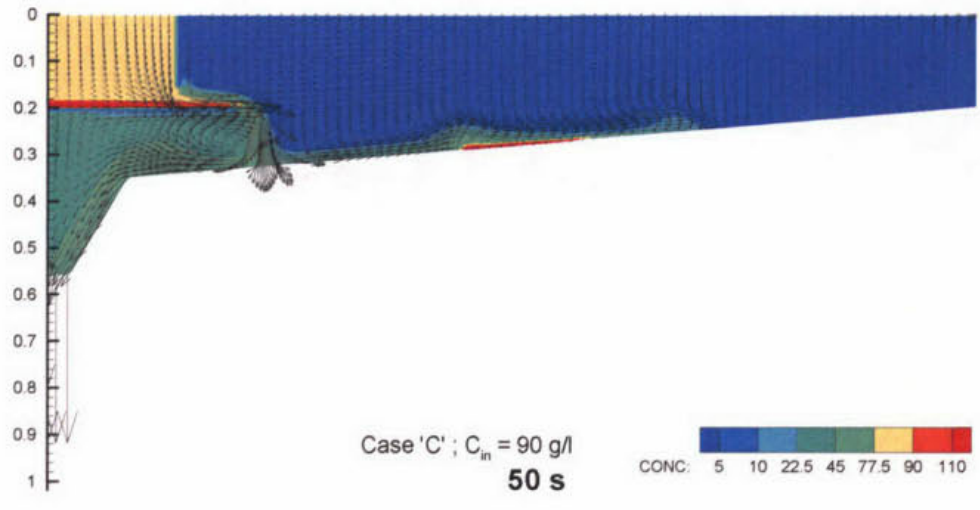

Fig. 7.16b

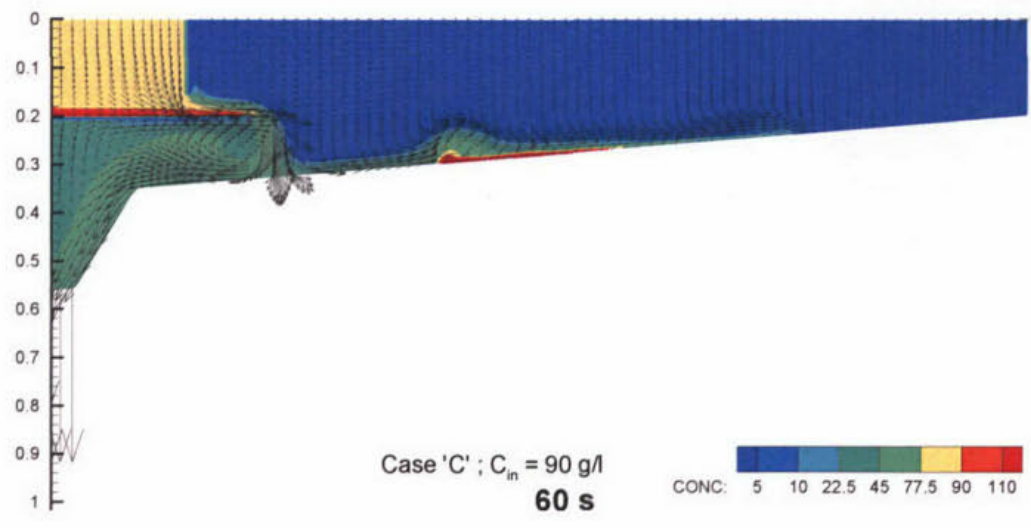

***Fig. 7.16c** Development of Counter Density Current*

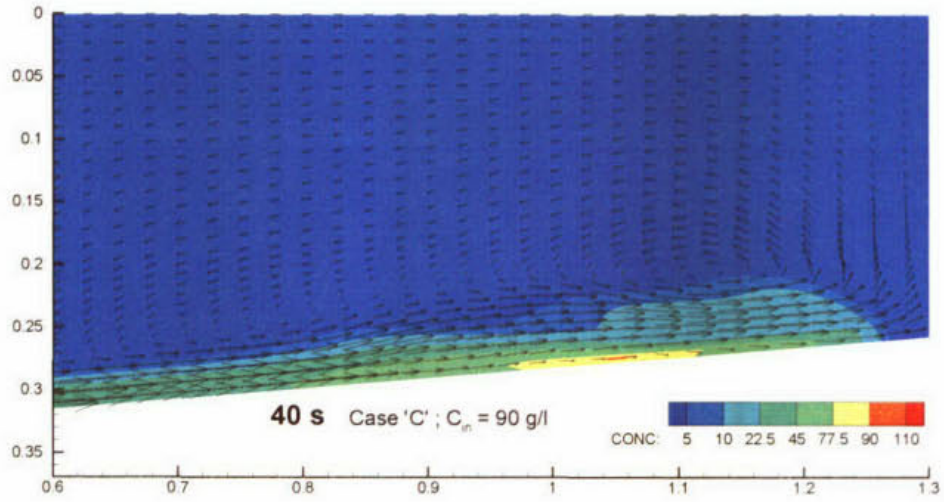

Fig. 7.17a

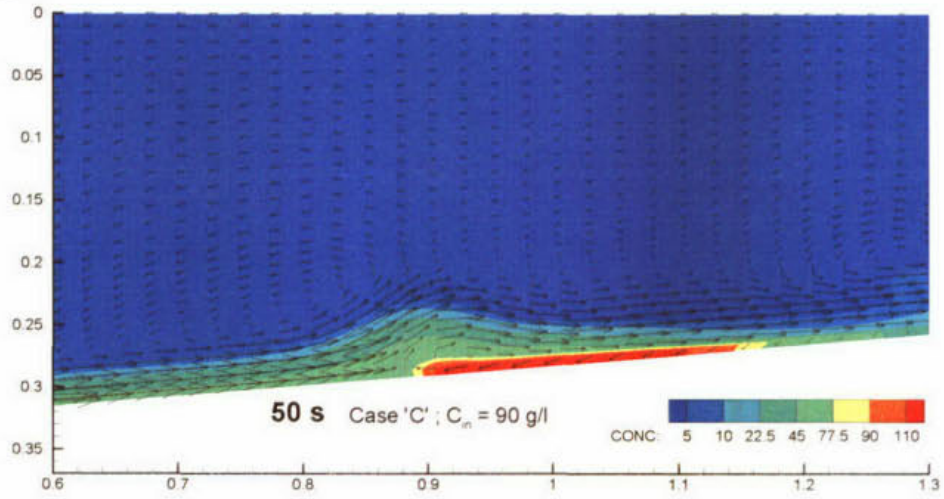

Fig. 7.17b

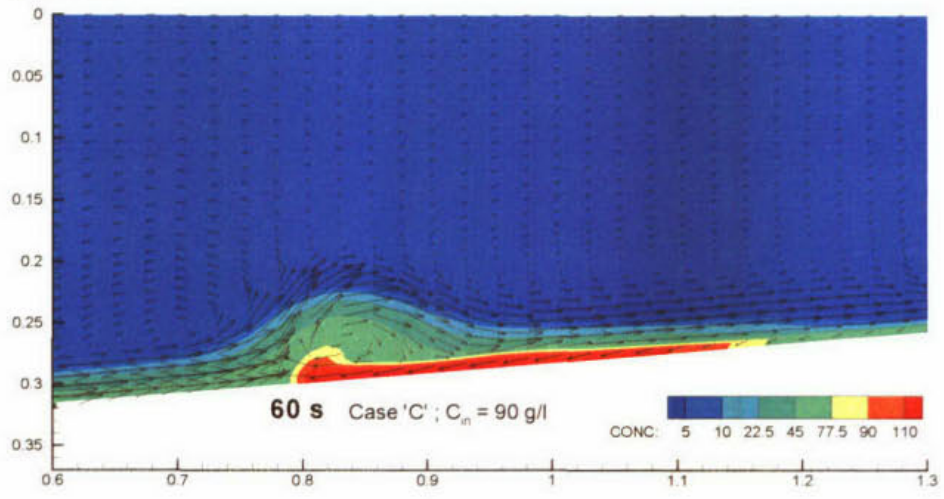

Fig. 7.17c *Starting at around 40 Seconds, a Counter Density Current develops along the Sloping Bottom. The Outward Flow separates from the Bottom and is directed upward*

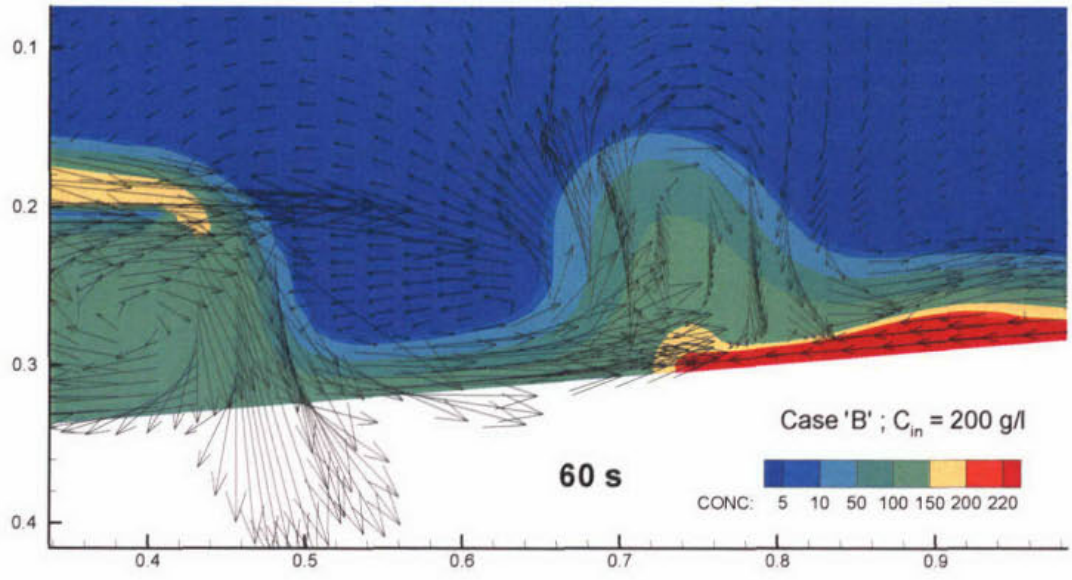

Fig. 7.18 a

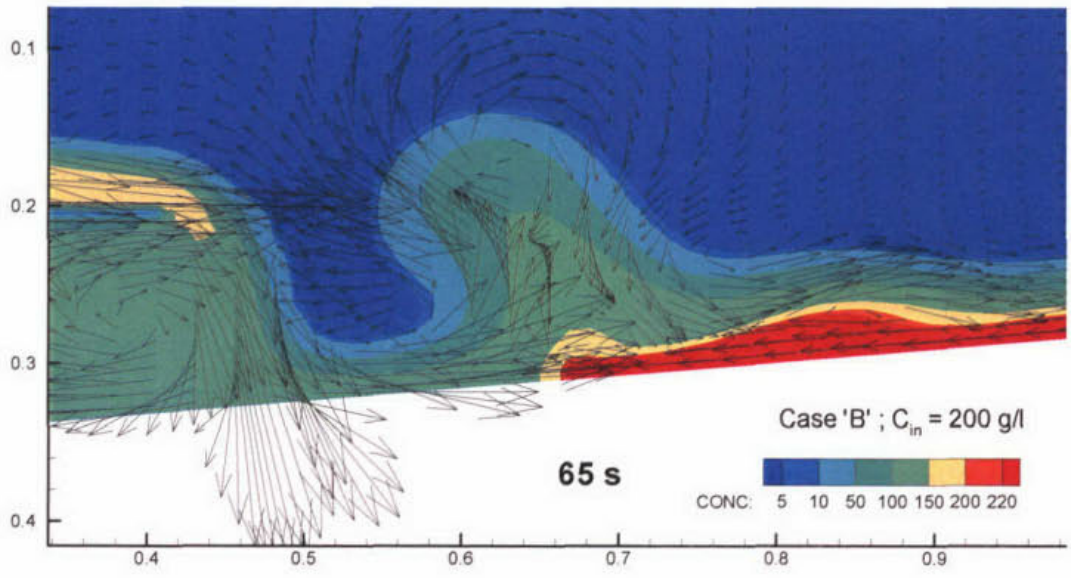

Fig. 7.18 b *Counter Density Current retards and temporarily stops the outward flow*

8 Conclusions

The initially planned experiments in which flow and sedimentation behaviour in a real secondary clarifier were to be simulated in a laboratory model and detailed measurements were to be performed were unfortunately not successful. The failure of the various attempts was mainly due to the fact that no artificial sludge to be used as model suspension could be found which had the flow properties of real activated sludge. As opposed to the latter, the model suspensions tested could not sufficiently easily flow out of the tank nor be scraped out of the tank once settled and compacted at the tank bottom . The conclusion therefore is that the processes in a real secondary clarifier cannot be simulated in a small-scale laboratory model.

There were further difficulties in obtaining reliable velocity and concentration measurements due to the very high concentrations and small velocities in the model tank dictated by the similarity laws. The purpose of generating experimental data for an extensive testing and validation of the numerical model could therefore not be reached and this validation must rely on measurements in prototype tanks.

One aspect of the numerical model could, however, be tested to a certain extent, and that is its ability to simulate the start-up phase when the loading is switched on and the suspension moves as a density current to the outer wall. Reasonably reliable information on this process could be derived from the measurements through visual observations of the suspension movement and hence the propagation of the current front. However, also in this situation the model sludge limited the usefulness of the experimental results because the mixture of Lewatit and iron hydroxide particles started to separate and the particles again stuck to the bottom and prevented any movement of settled material towards the sludge hopper as occurs in real tanks and was also predicted in the numerical simulations. A comparison of the simulations with the visual observations was therefore possible only for the very initial stage where this movement did not yet occur. In this stage it was found that the numerical model simulates altogether the unsteady start-up process fairly well.

9 References

Krijgsman J. (1996). *Internal Notes on STOWA-project.*

Lakehal D., Krebs P., Krijgsman J. and Rodi W. (1999). Computing shear flow and sludge blanket in secondary clarifiers. *J. Hydraulic Engng.,* ASCE, **125** (3), 253-262.

Mandersloot W.G.B., Scott K.J., Geyer C.P. (1986). Sedimentation in the hindered settling regime. *Advances in solid-liquid separation edited by H.S. Muralidhara, Betelle Press.*

Uliczka K. (1989). „Zur messtechnischen Erfassung des Sedimenttransportes unter Sheet-Flow-Bedingungen." *Leichtweiß-Institut für Wasserbau an der TU Braunschweig,* Sonderdruck aus Heft **105** (1989) der Mitteilungen

Simpson J. E. (1987). "*Gravity currents in the environmental and the laboratory.*" Ellis Horwood Ltd., Chichester, England.

Vogel, S. 1981. "*Life in Moving Fluids: the physical biology of flow.*" Boston, Mass.: Willard Grant Press.